DISTRIBUTIONS ACROSS THE PLUME OF TRANSVERSE LIQUID AND SLURRY JETS IN SUPERSONIC AIRFLOW

by

Russell H. Thomas

Thesis submitted to the faculty of the

Virginia Polytechnic Institute and State University

in partial fulfillment of the requirements for the degree of

Master of Science

in

Aerospace and Ocean Engineering

APPROVED:

Dr. J.A. Schetz, Chairman

Dr. W.F. O'Brien

Dr. A.K. Jakubowski

May, 1984

Blacksburg, Virginia

DISTRIBUTIONS ACROSS THE PLUME OF TRANSVERSE LIQUID AND SLURRY JETS IN SUPERSONIC AIRFLOW

by

Russell Hicks Thomas

(ABSTRACT)

Liquid and slurry jets were injected through a circular orifice transverse to a M = 3.0 airflow. Mass samples of both jets were taken across the plume 30 injector diameters downstream. Pitot and static pressure surveys were taken across the liquid jet. These data allowed the calculation of distributions across the liquid jet plume of Mach number, air mass flow, liquid-to-air ratio, and momentum flux. A correlation for the liquid concentration in the downstream plane is also presented. In the plume, there is a core region of subsonic airflow carrying two-thirds of the mass collected in the plume. In the core, the liquid mass flow is nearly constant from side-to-side at a given height, and the average velocity of the liquid is only 30 to 60% of the local air velocity. A supersonic mixing region covering two-thirds of the area of the plume surrounds the core region. Comparison with the results from this direct sampling data indicate that correlations developed from photographic techniques are inadequate in determining the jet penetration and width of liquid and slurry jets. The slurry jet showed substantial phase separation. A 30% mass-loaded slurry of

1-5 μm silicon dioxide particles mixed with water was injected, and the local loading varied from a low of 13% at the bottom of the plume to 100% outside the liquid plume. The local loading increased as the jet boundary was approached from any direction.

ACKNOWLEDGEMENTS

I am greatly indebted to Dr. Joseph A. Schetz, my advisor, for his guidance throughout the course of this research. The original concept for this study was his, as were the solutions to many of the problems encountered along the way. His consistent support made it possible for me to successfully complete this thesis. I certainly have profited from my association with Dr. Schetz.

I thank Dr. W. F. O'Brien and Dr. A. K. Jakubowski for serving on my committee and for providing excellent and motivating instruction to me as an undergraduate.

I extend my gratitude to Dr. Julian Tishkoff and the Air Force Office of Scientific Research for the financial support of this research.

I thank Dr. Felix Sebba of the Chemical Engineering Department for his permission to use valuable equipment which greatly improved the accuracy of the results of this research.

I greatly appreciate the outstanding technical support in the laboratory given by Mr. Gary Stafford, the expert machining done by Mr. Frank Shelor, Mr. Jake Frazier, and Mr. Kent Morris of the Aerospace machine shop, and the always helpful staff of Mrs. Pat Snider, Ms. Jeannie Gay, Mrs. Janice McCraw, Mrs. Marge Teates, and Mrs. Kim Padgett.

Lastly, I have my fellow students to thank, especially Mr. Dave Less and Mr. Brian Kemp for valuable assistance and discussion.

TABLE OF CONTENTS

LIST OF FIGURES

NOMENCLATURE

C_a	air concentration in plume
C_d	discharge coefficient
C_l	liquid concentration in plume
C_{l_m}	liquid concentration on the centerline
d	injector diameter
h	penetration of jet plume
h_{core}	penetration of jet plume core
M	Mach number
$\dot{m}_a/A$	mass flow of air per unit area
$\dot{m}_l/A$	mass flow of liquid per unit area
P_s	static pressure
P_{t1}	local free stream total pressure
P_{t2}	local Pitot pressure
$\bar{q}$	jet to free stream momentum ratio
R	gas constant for air
T_o	local total temperature
T_s	local static temperature
V_j	injectant velocity at injector
V_∞	free stream velocity
V_l	average velocity of liquid in plume
V_a	local velocity of air in plume
w	width of jet plume

w_{core}	width of jet plume core
x,y.z	rectangular coordinates, origin at injector
y_c	distance from centerline to y at $C_l = 1/2\ C_{l_m}$
ρ_∞	free stream density
ρ_j	injectant density
γ	ratio of specific heats

I. INTRODUCTION

The study of jets injected transverse to a supersonic gas cross-flow is a problem of both practical and theoretical interest. Such a process is encountered in thrust vector control, local re-entry body cooling, external burning on projectiles, control of vehicles and fuel injection into supersonic combustion chambers. Theoretical interest is derived from the complexity of the general problem which includes 3D, multiphase, unsteady, turbulent flow with subsonic and supersonic regions. Some applications also involve chemical reactions. This complexity also makes it prohibitive at this time to approach the problem from an entirely theoretical point of view requiring extensive basic experimental studies.

Past work has concentrated on the study of liquid injection. Much work has been done to develop correlations for jet penetration including the effect of injection angle (Refs. (1), (2), (3), (4)). All of these used photographic techniques to determine the penetration without determining how accurately this represented the actual penetration. The effect of liquid viscosity and surface tension on jet penetration were found to be minimal (Ref. (5)). However, Nejad and Schetz determined that these properties had significant effects on droplet diameter (Ref. (6)). A number of injector configurations were tested by Joshi and Schetz to determine the effects on jet penetration and spread (Ref. (7)). The improved atomization from injector combinations producing impinging jets has been documented by Hewitt and Schetz (Ref. (8)). The actual

process by which these jets breakup and atomize has been observed by Joshi, Kush and Schetz to be that of gross clump fracture (Refs. (9), (10)). These, along with other work, have concentrated on penetration, atomization, jet structure and breakup of liquid jets.

Fuels more energetic than conventional liquids have always been under consideration because of the potential gains in range and compactness. One attractive alternative is slurry fuels produced by suspending metal powders in liquid hydrocarbon carriers. The possible increase in heat of combustion is significant (Ref. (11)). Olson and Breitwiser describe many of the results of early NACA research in slurry fuels (Ref. (12)). The difficulty of boron slurry combustion was made evident. At locally rich fuel-air ratios, high enough local gas temperatures resulted in destruction of combustors yet at cooler temperatures significant deposition of boron oxides resulted along with unacceptably low combustion efficiencies.

Reference (13) describes recent advancements in boron combustion. Less and Schetz (Ref. (14)) have studied the injection of slurry fuels. That work examined the penetration and breakup of slurry jets injected transverse to a supersonic stream. They observed photographically that there was significant phase separation.

Good mixing of fuel and air is always important for efficient combustion in any system, but proper mixing of any type of fuel with the main airflow is imperative in supersonic combustion because of the very low residence times. This is the problem of primary interest here, and

its understanding is linked necessarily to a fundamental knowledge of jet structure, breakup, and plume characterizations. The previously mentioned research has contributed to the understanding of jet structure and breakup. However, distributions of important quantities in the plume has been a sparsely researched area for both slurry and liquid jets. Chinese researchers have determined, by direct sampling, fuel distributions for liquid transverse injection in subsonic streams (Ref. (15)). Soviet researchers using a temperature survey method indirectly determined the gas phase concentration inside a liquid jet injected transverse to a supersonic stream (Ref. (16)). Thus, the present research was designed to determine the first mass distribution by direct sampling in both a liquid and a slurry jet in supersonic airflow. This mass distribution combined with static and Pitot pressure measurements could then be used to calculate other important distributions in the jet plume such as injectant-to-air ratios. In addition, this information combined with new photographic observations provides possible links between the structure and breakup of the jets and the resulting plume distributions allowing further insight into the basic fluid mechanics of this complex problem.

II. EXPERIMENTAL APPARATUS AND METHODS

2.1 Test Facility

800 tests were conducted in the Virginia Tech 23 cm by 23 cm supersonic blowdown wind tunnel with Mach 2.4, 3.0, and 4.0 capability via interchangeable nozzles. All these tests used the Mach 3.0 configuration. The stagnation pressure was maintained at 4.5 atm $\pm$ 2%, and the stagnation temperature was that of outside ambient air (approx. 25°C). Run times were at least 15 seconds.

2.2 Injectant

Cost and safety considerations prohibited using hydrocarbon carriers and metallic solid fuels such as boron in this work. Water was used to simulate hydrocarbon fuels, and a mixture of water and silicon dioxide particles served as the slurry. No additives were included in the slurry mixture. The use of substitute injectants such as these are accepted practice for basic studies. The silicon dioxide particles have a density of 2.35 gm/ml and are of irregular shape thus approximating elemental boron. The particles were manufactured to a size range of 1-5 μm by Atlantic Equipment Engineers.

2.3 Injection System

A modified six liter chemical mixer was used to insure uniform mixing of the slurry. The tank was pressurized to 12 atm for slurry

injection with continuous mixing throughout the run. The paddle was driven by a 0.37 KW motor and turned at 60 rpm. For water injection the mixer was used as a reservoir pressurized to 17 atm.

For liquid injection, a drag-body type Ramapo meter was used. For the slurry tests, a Micro Motion C25 mass flow meter was used successfully with little trouble due to the absence of intrusive parts in the meter. A schematic of the injection system is shown in Fig. 1.

2.4 Flat Plate Model

The liquid and slurry were injected through a flat plate having dimensions 10.0 x 15.25 x 0.9 cm and a sharp leading edge. The plate was attached to the bottom of the test section by a 5.5 cm tall support. The circular injector orifice was located 8.0 cm downstream of the leading edge. The orifice had a conical entry passage and a diameter of 2.0 mm. It was the intent of this research to simplify this flow problem as much as possible by studying a basic configuration which could later be extended. Thus, the flat plate model was used to minimize the boundary layer and its effects. The flat plate model is shown in Fig. 2.

2.5 Photographic Methods

Two types of photographs were taken. First, a General Radio Strobotac was used as the light source for a Schlieren optical apparatus to take spark Schlieren photographs of the jets. The 10^{-6} second

exposure time with Type 57 Polaroid (ASA 3000) film provided an instantaneous shock shape and side view of the jet. Second, front lighted photographs provided unique views of the leading edge of the jets. Exposure times of 10^{-4} sec were used on Ektachrome ASA 64 film and were used with a commercially available Minolta X-700 35 mm camera with a Minolta 360 PX flash.

2.6 Sampling System

The sampling probe was designed to obtain true mass flow samples at supersonic speeds. The probe was connected to a vacuum system which created a pressure inside the probe lower than the total pressure behind the stand-off shock in front of the probe causing the shock to be swallowed into the probe. In this fashion, a streamtube equal in area to the probe capture area can enter the probe undisturbed. The internal probe diameter diverged from 1.20 mm to 5.1 mm causing one normal shock in the sampling tube (see Fig. 3). A 45 cm run of 5.1 mm ID tubing took the sample from the capture area to a three way valve outside the tunnel. The valve switched the sampling flow between a dummy sample bottle and a true sample bottle. The vacuum system established flow through the dummy bottle until steady conditions were reached. The valve then switched sampling flow to the true sampling bottle for 5 seconds and then back to the dummy well before any end-of-run transients. This allowed the mass flow of injectant for the given probe capture area to be

calculated. The sampling system is shown in Fig. 4.

Liquid jet samples were collected in 15 ml plastic bottles weighing approximately 5 grams, and in the slurry tests, 15 ml glass bottles weighing 13 grams were used. Each bottle was individually tared on a Mettler #33AR precision balance accurate to $\pm$ 0.0005 gm.

Slurry samples were weighed wet after collection and then heated at between 105°C to 130°C long enough to evaporate all the liquid carrier and then weighed again to determine the solid weight.

On the periphery of the slurry jet where solid particles had been thrown free of the liquid jet a filter system replaced the sample bottle. These were glass fiber Gelman Sciences filters of 0.7 μm pore size used in a Gelman 1190 filter holder.

2.7 Pressure Measurements

The pressure tap in the sampling probe was primarily intended to check flow conditions during sampling. The probe could also be used as a Pitot pressure probe by sealing the sampling tubing allowing no flow through the probe. In supersonic flow, the pressure measured was then the total pressure behind the normal shock in front of the probe, P_{t2}. This also permitted determining when the vacuum system could lower the pressure in the probe below this value in order to insure swallowing of the shock. However, due to the erosive nature of the slurry jet, the sampling probe had to be replaced four times and the pressure tap was also moved to the sampling bottle area.

A small flat plate 1.27 cm by 1.91 cm by 0.16 cm with a pressure tap on the surface and a sharp leading edge was used to measure static pressure in the liquid jet only. Thus, at each station total pressure behind the shock, P_{t2}, and the static pressure, P_s, could be taken. If the flow was not supersonic then the total pressure measured would be P_{t1}, the local free stream total pressure.

2.8 Test Matrix and Parameters

The primary similarity parameter used in injection studies is $\bar{q}$, defined as the jet to free stream momentum flux ratio ($\rho_j V_j^2 / \rho_\infty V_\infty^2$). A $\bar{q} = 6$ was chosen for the all-liquid jet tests and was maintained to within $\pm$ 1.7%. The corresponding mass flow rate was maintained at 90 gm/sec $\pm$ 1.1% throughout.

Figure 5 shows the coordinate system used. All data were collected in the x/d = 30 plane. Previous work has concluded that penetration due to jet normal momentum is complete at this downstream station (Ref. (9), (16)). Samples were taken in the -y/d, +z/d half plane at increments of 2d for the bulk of the data. Traverses at three values of z/d in the +y/d plane were made to check for jet symmetry. At each station, at least three samples were taken.

Solid loading of a slurry is defined as mass of solid divided by mass of the total mixture, and volume loading is defined similarly for volumes. A solid loading of 30% was chosen as a reasonable value for an exploratory study. Higher loadings (> 55%) produce complex changes in

the injectant flow from the orifice (see Ref. (14)), and it was decided to avoid those complexities in this work. The mass loading of 30% corresponds to a volume loading of 15.4% and a mixture density of 1.208 gm/ml which was maintained to within $\pm$ 1.5%. Since mass distributions were to be collected, it was felt that the mass flow of slurry should be matched with the all-liquid tests. For the slurry tests, the mass flow was maintained at 90 gm/sec $\pm$ 6.6% corresponding to $\bar{q} = 5 \pm 14.0\%$.

Again, most slurry sampling was done in the -y/d, +z/d half plane with two traverses in the +y/d half plane to check for symmetry. At least two samples were collected at each station. Greater margins in flow rate were allowed and fewer samples were collected in the slurry jet survey due to the increased cost, time and effort, and difficulty of performing slurry tests.

III. RESULTS

3.1 Jet Breakup

For liquid jet breakup in supersonic crossflow, three distinct regimes of jet behavior exist determined by injector diameter and more strongly by $\bar{q}$ (Ref. (9)). Regime 1 corresponds to low $\bar{q}$ and is characterized by minimal jet penetration. Of more interest for fuel injection are Regimes 2 and 3 because of their higher penetration. Regime 3 corresponds to very high $\bar{q}$. In this case the jet forms a smooth profile as it is turned by the crossflow, and surface waves are only perturbations in the basic jet shape (Ref. (9)). The surface waves grow and clumps detach regularly at troughs in the waves resulting in a relatively smooth jet shape. The clumps then atomize as they proceed downstream. For small circular injectors, d = 0.8 mm, Regime 3 begins at $\bar{q} > 6$, but for larger injectors, d = 1.6 mm, it begins for $\bar{q} > 5$ (Ref. (9)). Regime 2 for the 0.8 mm diameter injectors ranged from $\bar{q} = 1.5$ to 6 and from $\bar{q} = 1.2$ to 5 for the 1.6 mm injector (Ref. (9)). Regime 2 differs from Regime 3 in that the waves now determine the profile. These are large, steep waves which form close to the injector. These waves create steps early in the jet penetration; that is, the local inclination of the profile relative to the free stream is significantly altered, even becoming parallel temporarily to the free stream, before continuing to penetrate further. Thus, for the present research using a 2 mm circular injector, both the liquid and slurry jets with $\bar{q}$'s of 6 and 5

respectively would be expected to exhibit Regime 3 behavior.

A series of 21 spark Schlieren photographs for the liquid jets and 36 for the slurry jets shows that both smooth and stepped profiles are evident in both jets. Figure 6 gives two representative pictures of a smooth and a stepped profile for a liquid jet. Figure 7 shows corresponding pictures for a slurry jet. Thus, both jets showed the stepped profile characteristic of Regime 2 jets. More interestingly, 50% of the slurry profiles were stepped or 2.5 times more frequently as the liquid jet. In addition, the difference between the stepped and smooth profiles for the slurry jets was much more distinct than in the liquid jets. However, for both jets, the average height for the occurrence of a prominent step in the profile was 6d.

It is true, nevertheless, that the transition between Regimes 2 and 3 is a gradual one and, thus, it is possible that the slurry jet although strictly in Regime 3 may be too close to the transition region to exhibit purely Regime 3 behavior. It is also possible that slurry jet breakup regimes may occur over different $\bar{q}$ ranges. An examination of two more observations below will indicate which of these two possibilities is the more likely.

First, the authors of Ref. (14) also collected spark photographs of the same slurry used in this research at loadings of 33 to 36%. For a $\bar{q}$ range from 5.9 to 11.6, two of six pictures showed stepped profiles including one at $\bar{q}$ = 11.6. In the range of $\bar{q}$ from 2.8 to 4.7 three of five pictures also showed stepped profiles. Clearly, the stepped

profile is characteristic of slurry jets over a much wider range of $\bar{q}$ than is found in liquid jets.

Second, the stepped profile appears to be linked to an upstream-downstream oscillation of the jet body and, in general, seems to create a sooner, more violent breakup of the jet. This would probably result in smaller clumps and droplets downstream. The jet body is the continuous liquid portion of the jet before clumps have been detached. Reference (14) presented laser extinction tests which consisted of the time variation of the undiffracted laser beam intensity. Those tests were conducted for $\bar{q}$ = 7 slurry and liquid jets of 30 injector diameters downstream. Both jets showed the expected time variation in the intensity, but with the amplitude of the fluctuations for the slurry being on average 20% less than that for the liquid jet. This would occur if the droplets were smaller and had a more uniform distribution resulting from a more rapid violent breakup of a stepped profile. Apparently, the stepped profile breakup of the slurry jet noticed visually at lower $\bar{q}$ values might exist at $\bar{q}$ = 7. Thus, from all these observations taken together it might be concluded that slurry jets in a $\bar{q}$ range from 2.8 to 11.0 exhibit a stepped profile jet breakup which produces a more rapid atomization than in liquid jets. That is, Regime 2 slurry jet breakup appears to extend to a significantly higher $\bar{q}$ than in liquid jets.

It has been found that for Regime 3 liquid jets, an increase in viscosity of the injectant increases the droplet diameter and delays

the atomization of the jet to further downstream (Ref. (6)). This implies a fundamental difference with slurry jets which in general have very high viscosity, since the previous discussion concluded that slurry jets probably produced more uniform distributions of smaller particles. This difference is intuitively reasonable given the already discussed more violent breakup of the slurry jet, but also in that the particle-liquid interaction in a slurry could accelerate atomization. The source of the interaction is the different rates of acceleration by the local airflow on particles of different density.

3.2 Surface Layer

The surface layer is created by the interaction of the separation region around the injector, the boundary layer, and the jet column. On the surface of the flat plate liquid is drawn upstream for a short distance directly in front of the leading edge of the jet column. This liquid is then split into two strands which are swept downstream far on either side of the jet. A top view photograph (see Fig. 8) from Ref. (7) documents this primary surface layer.

Figure 9 is a front lighted photograph of liquid injection at $\bar{q}$ = 6.0. It clearly shows the primary surface layer, but also shows a substantial layer directly underneath the jet. Reference (9) has only mentioned briefly just the existence of this "wake" surface layer. Hundreds of runs at the same conditions were required in order to accomplish the mass flow distribution to be described shortly and the

result was that polished surfaces were left by the surface layer. These are sketched in Fig. 10. The measured width from the mass distribution at x/d = 30 is 20d and using this with the observation that the half angle of divergence is 16°, which is roughly constant for liquid jets of $\bar{q} > 4$ (Ref. (9)), the rough boundary of the jet from the top view is sketched in Fig. 10. It clearly shows that the wake surface layer is obscured by the jet body. Previous research (Ref. (7), (9)) have used only top view photography to observe the layer and, thus, this has gone undocumented. The half angle of divergence of the two strands that make up the wake liquid layer is 8° or half that of the main jet body.

A much more defined pattern is documented in Fig. 11 after one hundred slurry runs at $\bar{q} = 5$ because of the much more erosive nature of the slurry. Only a trace of a primary layer was noticed in contrast to the larger primary layer of the liquid jet. However, a relatively heavily eroded region corresponded to the wake surface layer. Again, using the known width at x/d = 30 the half angle of divergence of the slurry jet body can be no more than 9°. This is in sharp contrast to the relatively constant 16° found for liquid jets. Below $\bar{q} = 4$, liquid jets diverge at angles between 9 and 13° before being swept downstream at a constant width (Ref. (9)). This could be the case for the slurry jet in which case it might indicate that Regime 2 extends to beyond $\bar{q} = 5$ for slurry jets as has been discussed in the previous section. Furthermore, the half angle of divergence of the eroded strands of the wake layer was 20°, more than twice that for the liquid jet.

The front lighted photographs also show that there is considerable transfer of mass from the plume to the surface downstream of the injector. This together with the significant erosion patterns appears to indicate that a significant percentage of the injected mass flow may be carried in the surface layer.

3.3 Jet Leading Edge

Previous research has shown that high frequency, large amplitude, aerodynamically-induced waves that ultimately result in gross fracture of the jet body begin to grow on the leading edge of the jet soon after exiting the injector (Ref. (9)). The front lighted photograph of Fig. 12 shows a cone shaped liquid core just at the exit of the injector. Its height is about one injector diameter. At this height, liquid begins to be sheared off the sides of the jet to form spray. However, the leading edge remains liquid for an additional 3d to 4d for a total height of 4d to 5d. This is the leading edge wave strip where the waves mentioned above are formed. The strip is obscured on either side and beyond a height of 4d to 5d by spray and/or clump formation. Pictures of the slurry jet do not reveal the core or wave strip (see Fig. 13). However, this is probably due to the low contrast between the opaque, white slurry and the white appearing spray. Visual observations, which can be more discerning, indicate that the slurry exhibits a similar structure.

It is interesting to note that the wave strip height of 4d to 5d

is just below the average height of the steps, 6d, observed in the spark Schlieren profiles. In addition, the height of the wave strip is also close to the sonic angle location for these conditions. The sonic angle is defined as the point on the bow shock where immediately downstream of this point the flow is sonic. This occurs since the bow shock is initially normal and as the jet is turned by the flow the bow shock becomes oblique. The transition to supersonic flow changes the wave nature on the jet to a longer wavelength type which later produces jet body fracture (Ref. (9)). This transition obviously creates a spray which obscures the wave strip as seen in the front lighted photographs. At M = 3 the sonic angle is 64°. The vertical distance to the location of the sonic angle was in the range 5d to 6d from spark Schlierens such as Fig. 6. For Regime 2 jets the steps in the profiles occur near the sonic angle (Ref. (9)). It is apparent that this is true for Regime 3 jets when step profiles occur.

The combined picture of a wave strip with surface wave growth and spray formation off the sides of the jet indicate that perhaps a circulation pattern in a kidney-shaped cross section exists similar to that noticed in subsonic jets and represented by a reproduction from Ref. (17) in Fig. 14. This pattern might persist downstream and be noticeable in the plume distributions to be presented shortly.

3.4 Liquid Sampling

The results of the sampling for the all-liquid jet case are presented in Fig. 15 in terms of mass flow per unit area [gm/sec mm^2]. This is one half of the x/d = 30 plane of the jet. Figure 15a shows the shape of the distribution and Fig. 15b lists the numerical values.

The actual cross-stream penetration of the jet at this station and how it compares with penetration estimates as compiled from photographic techniques is the first result. It can be seen that trace amounts of samples were collected at 19 injector diameters high, but, considering these as negligible, z/d = 18 could be called the penetration. Samples at z/d = 18 are roughly 4.0% of the maximum sample size on the centerline y/d = 0. Yates and Rice (Ref. (1)) obtained the following empirical equation for water penetration from a circular injector into a Mach 3.0 crossflow,

$$\frac{h}{d} = 1.15(\bar{q})^{1/2} \ln[1+6\ x/d].$$

At x/d = 30 and $\bar{q}$ = 6 this yields h/d = 14.6 or 19% below the actual penetration of h/d = 18. It can be noted that the point of maximum $\dot{m}_l/A$ is z/d = 12 or two-thirds the value of maximum penetration. Fig. 15b also allows the width of the jet at z/d = 30 to be determined. The data show that by y/d = -10, $\dot{m}_l/A$ is generally under 6% of the centerline value at that value of z/d. Joshi and Schetz (Ref. (7)) give the following expression for jet width

$$w/d = 11.2(\bar{q}C_d)^{0.19}$$

with an insignificant pressure term ignored. For circular injectors, $C_d \simeq 1.0$ and for $\bar{q} = 6$ Joshi's formula yields w/d = 15.8 or 21% below the present value of w/d = 20. Thus, photographic techniques seriously underestimate the dimensions of the liquid jet plume. This compares favorably with the results of Ref. (18) which concluded that the error in determining the plume boundary from photographic techniques could be 25-30%. Ref. (16) using a temperature survey method presented the following correlations for jet penetration and width:

$$h/d = 3.75(\bar{q})^{.414}(x/d)^{.239}$$

and

$$w/d = 13.8\ \bar{q}^{.25} \quad \text{at } x/d = 30.$$

These yield values of h/d = 17.8 which are negligibly different from the present value of 18 and w/d = 21.6 or 8% above the present value of 20. These values are in good agreement and demonstrate the importance of direct measurements.

From z/d = 2 to z/d = 10 the mass flow is relatively constant at each z/d station from y/d = 0 to y/d = -4 before dropping sharply toward the boundary. This identifies a core region with constant mass flow at a given z/d station. This core occupies approximately 1/3 the area of the jet plume. A region has been drawn in Fig. 15b which encloses the peak values of mass flow at each value of y/d. Apparently this region is the now co-flowing remnant of a kidney shaped cross section in the jet body indicating that indeed such a cross section may exist as was

postulated previously. Most of this region is within the jet plume core implying that the jet body determines the characteristics of the plume core region.

An integration of the mass flow across the x/d = 30 plane from the sampling data resulted in a mass flow of 67 gm/sec or 75% of the mass flow through the injector. As has already been discussed there is considerable evidence to indicate that the mass flow in the surface layer accounts for a considerable portion of the remaining mass flow.

Figure 16 shows two pieces of information. The first is the difference between the high and low values of $\dot{m}_1/A$ for the samples taken at each station or the "spread". Second, this number is expressed as a percent of the average of $\dot{m}_1/A$ at each station from Fig. 15b. The spread data show no clear pattern except that it becomes a large percentage of the average $\dot{m}_1/A$ as the boundaries of the jet are approached. This probably indicates unsteadiness at the plume edges. From pictures such as in Fig. 6, one can see that there is clearly unsteady behavior of the jet boundary. This motion is at very high frequencies on the order of 10^4 cycles per second (Ref. (10)). This type of behavior should not affect a 5 second sampling run. However, there may also be low frequency oscillations of the jet in both the upstream-downstream and side-to-side directions due, for example, to instability of separation zones surrounding the jet column at the injector. This instability is evidenced by large variations in the size of the interaction shock at the injector as seen in the spark Schlieren photographs presented.

3.5 Liquid Jet Symmetry

Jet symmetry and repeatability of the results were checked carefully. Figs. 17a, b, c show the data for three z/d levels in addition to data taken in the +y/d plane and some repeated sets of data in the -y/d plane. Two points can be made. First, when the data was repeated, values are within $\pm$ 10% and the spreads are generally overlapping. Second, these three sweeps show some asymmetry about y/d = 0 with symmetry about any other value of y/d not apparent. This observation could also add credibility to the speculation of a low frequency oscillation of the jet.

3.6 Slurry Sampling

Figure 18 shows data taken in the x/d = 30 plane for the nominally 30% loaded slurry jet. Both the average local particle loading of the samples and the total mass flow per unit area are shown. The loading increases smoothly in the +z/d direction from z/d = 2 to z/d = 10 then jumps sharply at z/d = 12 to almost triple the value at z/d = 2. This increased loading is due to the heavier particles following paths with greater radii of curvature due to their greater inertia and thus separating from the liquid plume consistent with the visual observations of Ref. (14). Perhaps unexpectedly the same phase separation was noticed side-to-side in the -y/d direction at both z/d = 2 and z/d = 10. The same trend was evident in the +y/d direction at the same z/d values as

is shown in Fig. 16. Some asymmetry of the slurry plume is also evident in mass flow and to a lesser extent in the loading results.

The magnitude of the spread in the results and its percentage of the average are shown in Fig. 19. The same conclusions made for the liquid jet data can be made here. The same indication of unsteadiness of the boundary was also noticed. Beyond the slurry boundary samples of dry particles were collected using the filter system described previously. At z/d = 14, y/d = 0 samples of negligible weight were collected on only one-third of the runs. At z/d = 10, y/d = +8 samples were collected three-quarters of the time but at z/d = 10, y/d = -8 the rate was only one-fourth. Again this indicates some low frequency oscillation of the jet boundary.

The sampling data defines the penetration at h/d = 12. This is 13% below the Yates and Rice correlation value of 13.6 for these conditions although it must be considered that the correlation was developed for liquids only. Ref. (14) determined the penetration for an identical slurry using photographs at h/d = 13, also high. However, solid alone will penetrate at least 16% higher occasionally to z/d = 14. The width of the slurry jet, w/d = 12, is also overestimated by the Joshi correlation by 25% at w/d = 15.2. The formulas of Ref. (16) which were developed for liquid jets and compared very well with the present liquid plume measurements would overestimate the penetration of this slurry jet by 37.5% and the width by 71.6%. Clearly new correlations for width and penetration must be developed for slurry jets.

3.7 Pressure Distributions

The total pressure data distribution in the all-liquid jet is shown in Fig. 20a. The static pressure, P_s, is given in parentheses above total pressure measurements in Fig. 20b. Also shown is the average time variation in the total pressure during a run.

The flat plate probe used to measure the static pressure was found to measure the static pressure in the free stream about $2.07 \times 10^3 N/m^2$ too high due presumably to a slight angle of attack (this is detailed in the Appendix). Nevertheless, the static pressure measurements in the water jet are presented as collected. The static pressure varied by less than 3.45×10^3 N/m^2 within the jet and differed by less than 3.45×10^3 N/m^2 from the free stream static pressure of about 1.16×10^4 N/m^2.

The total pressure measurements show considerable variation from low values in the center to free stream values on the boundaries. The time variation of total pressure measurements shows a clear pattern. Relatively large time variations are evident along the boundary of the jet while no variations were measured in the center region. This could be more evidence for jet oscillation of the order of 1 cycle per second, a frequency which could affect the sampling data as stated before.

3.8 Mach Number Distribution

The Rayleigh Supersonic Pitot formula allows the calculations of the local free stream Mach number once P_{t_2}, P_s and γ are known:

$$\frac{P_s}{P_{t_s}} = \frac{\left(\frac{2}{\gamma+1} M^2 - \frac{\gamma-1}{\gamma+1}\right)^{1/\gamma-1}}{\left(\frac{\gamma+1}{2} M^2\right)^{\gamma/\gamma-1}}$$

This assumes supersonic flow and a known γ . If the flow is not supersonic then M is determined from:

$$\frac{P_{t1}}{P_s} = \left(1+\frac{\gamma-1}{2} M^2\right)^{\gamma/\gamma-1}$$

Simple calculations assuming uniform distribution of liquid droplets across the jet plume area show that there is only 0.0001 mm^3 of liquid per mm^3 of jet volume. At these low static temperatures, little liquid injectant vapor can be expected. Thus, the flow is primarily air, and for estimating M inside the jet, γ for air can be reasonably assumed.

The result is shown in Fig. 21. The values on the boundary are high as expected and do not exceed M = 3.0. The Mach numbers decrease smoothly as the center of the jet is approached to quite low values. There is actually a large subsonic region even though this is measured at x/d = 30 with a high free stream Mach number. This subsonic region should not affect the validity of the samples in that region since pressures in the probe during sampling were very close to local static pressure making the samples nearly iso-kinetic.

3.9 Jet Plume Core Region

Reference (16) concluded that there were two regions in the jet plume, a peripheral mixing region and an inner core region. From their temperature survey method they characterized the core region as where the measured temperature varied little and the mixing region by marked changes in temperature. Reference (16) obtained the following correlation for the penetration of this core region:

$$h_{core}/d = 3.17(\bar{q})^{0.414}(x/d)^{0.239}.$$

For the present test conditions this would yield a value of h_{core}/d = 15.0. Figure 15b shows similar trends for the liquid jet plume. As stated previously there is relatively constant mass flow from y/d = -4 to 4 at a given z/d station up to z/d = 12. Figure 16 indicates that this region has low run-to-run variation or relatively steady mass flow. Figure 20b shows the core region has virtually constant total pressure with no time variation in total pressure. This region also corresponds to the subsonic region as shown in Fig. 21. Thus, there is a clearly defined core region, however, at x/d = 30 its penetration is only h_{core}/d = 12 or 25% below the value from the less direct temperature method. The present data also gives w_{core}/d = 8 for the liquid
The core region also carries approximately two-thirds of the plume mass flow at x/d = 30 or one-half of total mass flow through the injector while it occupies only one-third of the plume area. Although the data for the slurry jet is not as complete the results in Fig. 18 would indicate that h_{core}/d = 10 and w_{core}/d = 4.

3.10 Liquid-to-Air Ratio

Figure 22 gives the static temperature distribution calculated using the Mach number from Fig. 21 as

$$T_s = \frac{T_o}{1 + \frac{\gamma-1}{2} M^2}$$

The argument for using γ for air has already been presented and found to yield reasonable results in the Mach number survey. The stagnation temperature, T_o, is taken as constant at 300°K, that of the free stream, since the shock or jet should not affect T_o. Thus, with the local values known the isentropic formula for T_s can be used. With this determined the mass flow of air per unit area can be calculated as

$$\frac{\dot{m}_a}{A} = M P_s \sqrt{\frac{\gamma}{R T_s}}$$

The assumption of a perfect gas is again valid because of the low pressures and the negligible evaporation. All of these quantities are known locally and the result is shown in Fig. 23. The minimum values of $\dot{m}_a/A$ are reached almost uniformly at z/d = 8 for all y/d values. The air mass flow increases sharply for z/d > 8 but also increases slightly for z/d < 8. An equivalent trend for $\dot{m}_l/A$ is not noticed as $\dot{m}_l/A$ drops smoothly toward the surface of the flat plate at z/d = 0.

The two mass flow distributions can be combined into a liquid-to-air ratio distribution which is shown in Fig. 24. For a typical hydrocarbon fuel, which these liquid tests simulate, stoichiometric

fuel-to-air ratio would be approximately 0.067. In addition, at low static pressures the flammability region would exist in only a narrow band around the stoichiometric value. As can clearly be seen, this condition would occur only in a very narrow band on the periphery of the jet where static temperatures will be lowest and Mach numbers will be highest - both complicating factors for combustion problems.

3.11 Momentum Flux

The velocity of the air, $V_a = M \sqrt{\gamma R \ T_s}$, is used to calculate the momentum flux of air per unit area, $\dot{m}_a V_a / A$, and both are shown in Fig. 25. Fluxes are seen to drop by about one order of magnitude from the supersonic region to the plume core. This is due to both lower velocity and lower mass flow of air. To calculate an equivalent momentum flux for the liquid an average velocity of the particles would have to be assumed. Certainly the velocity can be no greater than that of the air, but it could be equal to that of the air this far downstream. Momentum fluxes calculated on this assumption showed, however, that for the plume core region the momentum flux of liquid would be greater than that of the air which could not be since the liquid was injected with no axial momentum. Thus, in this region, the air momentum flux can be taken as a limit on the flux of the liquid. As such it can also give an upper limit on the velocity of the particles. In Fig. 26, the maximum velocity of the liquid expressed as a percentage of the air velocity at the same location is also shown. At least in this subsonic region, the

particles can be traveling at substantially lower velocities than the surrounding air even though this is at the x/d = 30 plane in a M = 3.0 flow. Previous work in a M = 2.0 flow assumed velocity equilibration to within 1% in the vicinity of the injector (Ref. (19)). Together, these two momentum flux distributions indicate that even though the jet has lost its normal momentum and is co-flowing with the air stream there is considerable momentum left to be transferred to the particles and air in the subsonic region from the surrounding supersonic region and possibly from the air to the droplets in the supersonic region also. Considerable mixing within the jet will occur for a large distance downstream.

3.12 Liquid Concentration Correlations

A correlation for the non-dimensional liquid concentration in the downstream plane of x/d = 30 can be derived as follows. The gas concentration is defined as

$$C_a = \frac{\dot{m}_a/A}{\dot{m}_a/A + \dot{m}_l/A}$$

and the liquid concentration by

$$C_l = \frac{\dot{m}_l/A}{\dot{m}_a/A + \dot{m}_l/A}$$

thus, the liquid and gas concentrations are related by

$$C_a + C_l = 1.$$

Values on the centerline, y/d = 0, can be denoted by the subscript m. Also, at a given height z/d the distance from the centerline to a point is y and y_c is the distance from the centerline to the point at which $C_l = 1/2\ C_{l_m}$. The data in the x/d = 30 plane is plotted as C_l/C_{l_m} vs. y/y_c in Fig. 27.

Reference (16) using an indirect temperature technique performed a similar correlation but for the concentration only in the plane of symmety, y/d = 0, for the plume at various x/d stations. The result was the equation

$$\frac{C_l}{C_{l_m}} = \left[1 - \left(\frac{Z}{2.01\ Z_c} \right)^{1.5} \right]^{1.6}$$

where C_{l_m} was the concentration on a centerline which connects the points of maximum liquid concentration at each x/d plane downstream of the injector. Simply written in terms of y coordinates and applied to the current data in the x/d = 30 plane it does not represent the data well as can be seen from Fig. 27. The data can be fit well by the cubic equation

$$\frac{y}{y_c} = -8\left(\frac{C_l}{C_{l_m}} - 1/2 \right)^3 + 1$$

although the slope at $y/y_c = 1.0$ is perhaps too high. In the absence of further data, this can be taken as an adequate representation for a wide range of downstream stations.

3.13 Liquid Jet Synthesis

As a means to synthesize the many aspects of the liquid jet structure, breakup and plume characteristics which have been investigated and described, Fig. 28 is presented as a schematic of the flowfield structure of a $\bar{q} = 6.0$ liquid jet.

IV. CONCLUSIONS

This research has contributed data to a sparsely researched area for transversely injected jets into supersonic flow - a mass flow distribution across the jet plume. The conclusions discussed below will hopefully add new insight to jet structure and mixing for both liquid and slurry injectants.

The actual penetration and width of the all-liquid jet at x/d = 30 were approximately 20% above that determined from photographic techniques. A favorable comparison with the published data of another intrusive method indicate that intrusive techniques provide a more accurate determination of jet boundaries. The correlations for liquid jets, however, are not applicable to the penetration and width of slurry jets.

Mass flow data indicate that the slurry and liquid jets are both slightly asymmetrical about the centerline axis. This along with additional sampling, pressure, and photographic data indicate that there is a possibility of low frequency oscillations of the jet in the side-to-side and upstream-downstream direction.

The leading edge of a liquid or slurry jet has been found to have a leading edge wave strip at least 4d to 5d high with droplet shearing off the sides. The height of the wave strip is linked to the location of the transition to supersonic flow over the jet. The circular jet probably is distorted early in its penetration into a kidney shaped cross section which is still identifiable far downstream affecting plume

distributions of mass flow.

A liquid-to-air ratio distribution calculated in the x/d = 30 plane of the liquid jet showed that for simulated fuel and air mixing at least one order of magnitude more air must be mixed with the liquid to bring ratios close to stoichiometric for a hydrocarbon-air mixture. A correlation for the non-dimensional liquid concentration across the plume at a downstream plane has been developed relating the non-dimensional distance from the centerline to the cubic of the concentration.

The cross section of the jet plume has at least two clearly defined regions. There is a core region which has high subsonic air velocity and a relatively constant mass flow in the side-to-side direction at a given vertical location along with low total pressure. The largest clumps detached from the main jet body form this core region. As a result, for the liquid jet at 30 injector diameters downstream the core occupies one-third of the plume area but carries two-thirds of the plume mass flow. The slow acceleration of these large clumps by the subsonic airflow results in the liquid particles having reached only 30 to 60% of the velocity of the air.

Surrounding the core region is the peripheral mixing region characterized by supersonic velocities, increasing Pitot pressures and decreasing mass flows. The remaining one-third of the mass flow captured in the plume is carried in this region. Droplets sheared off the sides and top of the main jet body and clumps is the source of the mass flow of this region. However, because of the high velocity and high air mass

flow in this region compared to that in the core region, considerable further mixing with and momentum transfer to the core region is anticipated downstream.

A similar structure in the slurry jet is likely. More importantly, substantial phase separation was found. The local loadings in the center of the jet was only one-third of the injected value and increased significantly as the boundary of the plume is approached from any direction.

For a slurry and a liquid jet of equivalent mass flow and $\bar{q}$'s of 5 and 6 respectively the breakup of the slurry was more violent and occurred sooner than the liquid jet. This resulted from a 2.5 times greater occurrence of a stepped jet profile as opposed to a more uniform profile. This breakup process is similar to that of Regime 2 liquid jets which occurs for a lower range of $\bar{q}$ from 1.2 to 5. For slurries, Regime 2 could extend as high as $\bar{q} = 11$.

At least two fundamental differences in jet structure exist between slurry and liquid jets at the tested conditions. First, the half-angle of divergence of the slurry main body is roughly half that of the liquid jet. This is apparently true also for slurry and liquid jets of equivalent $\bar{q}$. Second, the wake surface layer of the slurry has a half angle of divergence 2.5 times that of the liquid.

REFERENCES

1. Yates, C. L. and Rice, J. L., "Liquid Jet Penetration," Research and Development Programs Quarterly Report, U-RQR/69-2 Applied Physics Laboratory, Johns Hopkins Univ., 1969.

2. Kolpin, M. A., Horn, K. P. and Reichenbach, R. E., "Study of Penetration of a Liquid Injectant into a Supersonic Flow," AIAA J., Vol. 6, No. 5, May 1968, p. 853.

3. Forde, J. M., Molder, S. and Szpiro, E. J., "Secondary Liquid Injection into a Supersonic Airstream," J. Spacecraft, Vol. 3, Aug. 1966, p. 1172.

4. Catton, I., Hill, D. E. and McRae, R. P., "Study of Liquid Jet Penetration in a Hypersonic Stream," AIAA J., Vol. 6, No. 11, p. 2084.

5. Reichenbach, R. E. and Horn, K. P., "Investigation of Injectant Properties on Jet Penetration in a Supersonic Stream," AIAA J., Vol. 9, No. 3, March 1971, p. 469.

6. Nejad, A. S. and Schetz, J. A., "Effects of Properties and Location in the Plume on Droplet Diameter for Injection in a Supersonic Stream," AIAA J., Vol. 21, No. 7, July 1983, p. 956.

7. Joshi, P. B. and Schetz, J. A., "Effect of Injector Geometry on the Structure of a Liquid Jet Injected Normal to a Supersonic Air Stream," AIAA J., Vol. 13, No. 9, September 1975.

8. Hewitt, P. W. and Schetz, J. A., "Atomization of Impinging Liquid Jets in a Supersonic Crossflow," AIAA J., Vol. 21, No. 2, Feb. 1983, p. 178.

9. Kush, E. A. and Schetz, J. A., "Liquid Jet Injection into Supersonic Flow," AIAA J., Vol. 11, No. 9, September 1973.

10. Schetz, J. A., Kush, E. A. and Joshi, P. B., "Wave Phenomena in Liquid Jet Breakup in a Supersonic Crossflow," AIAA J., Vol. 18, No. 7, 1980, p. 774.

11. Olson, W. T. and Setze, P. C., "Some Combustion Problems of High-Energy Fuels for Aircraft," 7th Symposium (Int.) on Combustion, Butterworth Scientific Publications, 1959, pp. 883-889.

12. Olson, W. T. and Breitwiser, R., "NACA Research on Slurry Fuels Through 1954," NACA RM E55B14, 1954.

13. King, M. K., "Ignition and Combustion of Boron Particles and Clouds," J. Spacecraft and Rockets, Vol. 19, No. 4, July-August 1982, p. 294.

14. Less, D. and Schetz, J. A., "Penetration and Break-Up of Slurry Jets in a Supersonic Stream," AIAA J., Vol. 21, No. 7, July 1983.

15. Yang, M. L., Gu, S. J., Liu, G. E., and Li, X. Y., "Trajectory with Diffusion Method for Predicting the Fuel Distribution in a Transverse Stream," AIAA Paper No. 83-0336.

16. Shaikhutdinov, Z. G. and Klevanskii, V. M., "Penetration and Mixing of Liquid Injected into Supersonic Transverse Gas Stream," Izvestiya VUZ, Aviatsionnaya Tekhnika, Vol. 19, No. 1, 1976, pp. 99-108.

17. Abramovich, G. N., "The Theory of Turbulent Jets," M.I.T. Press, 1963.

18. Shaikhutdinov, Z. G., Klevanskii, V. M., Nadyrshin, A. Ya. and Shaikhinurova, L. F., IVUZ, Aviatsionnaya Tekhnika [Soviet Aeronautics], No. 4, 1973.

19. Edelman, R. B., Schmotolochen, S. and Slutsky, S., "Combustion of Liquid Hydrocarbons in a High-Speed Airstream," AIAA J., Vol. 9, No. 7, July 1971, p. 1357.

APPENDIX

ERROR ESTIMATION

Static Pressure Measurements

The static pressure measurements taken in the liquid jet are probably high by a maximum of 20 to 25%. This was found by comparing the measured free stream static pressure to the calculated free stream static pressure. The large percentage results from the low absolute values of static pressure. This error was probably caused by a -3° angle of attack of the flat plate static pressure probe. This being the probable source and magnitude of the error it is probably uniformly applicable to all static pressures in the liquid plume except for the fact that there are very small local inclinations of the flow in the plume.

Pitot Pressure Measurements

The major source of error involves the transfer of the momentum per unit area of the liquid particles entering the Pitot probe to the air. Thus, using the local velocity of the air as the maximum possible velocity of the liquid particles the momentum of the liquid divided by the capture area of the probe represents the maximum error in the total pressure measurements. This error is expressed as a percentage of the measured Pitot pressure. The results can be summarized into two groups. For Mach numbers greater than 2.0 the measured Pitot pressure was at

most 1.5% too high and on average 0.9% too high. For Mach numbers less than 1.5 the measured Pitot pressure was high by a maximum of 15% and on average about 8% too high.

Mach Number

Since the Mach number is a function of static and total pressures measured the error in the Mach numbers presented is a function of the errors just discussed. The errors in static and Pitot pressure tend to offset and thus the calculated values of Mach number in the subsonic region are at most 10% too low and in the supersonic region are at most 5% too low.

Mass Flow of Air

The mass flow of air was calculated from measured values. The error would result from the errors in Mach number and static pressure. Using the maximum errors possible for these two quantities it was calculated that the presented values of mass flow of air per unit area were at most 13% too high.

Mass Flow of Liquid

The balance error from weighing the samples was $\pm$ 0.0002 gm/s-mm^2 for the liquid mass flow per unit area and $\pm$ 0.0003 gm/s-mm^2 for the slurry samples. The larger error for the slurry is due to the extra weighing after heating of the slurry sample.

Misalignment of the sampling probe with the flow is also a possible source of error. A probe misalignment greater than 5° is unlikely and from the geometry would result in a 1% loss in captured mass flow from the loss in effective capture area.

The largest uncertainty, however, involved the operation of the probe in the subsonic portion of plume. Two flow scenarios are possible. It is possible to have a choking condition at the capture entrance to the probe followed by a supersonic expansion before a normal shock. Another possibility is for separation to occur at the entrance or shortly thereafter. The latter scenario is more likely when considering the sharp entrance and 22° divergence angle. In either case some distortion of the flow in front of the probe will exist. In the worst case where M = 0.6 with choked flow at the entrance the maximum increase in effective capture area over the capture area of the probe is 17%. Thus at most the values of $\dot{m}_1/A$ are 17% too high in the subsonic region.

Furthermore, any evaporation of liquid in the sampling probe is unlikely because of the low vapor pressure of water at room temperature. Checks for condensed water in the sample collection system confirmed this.

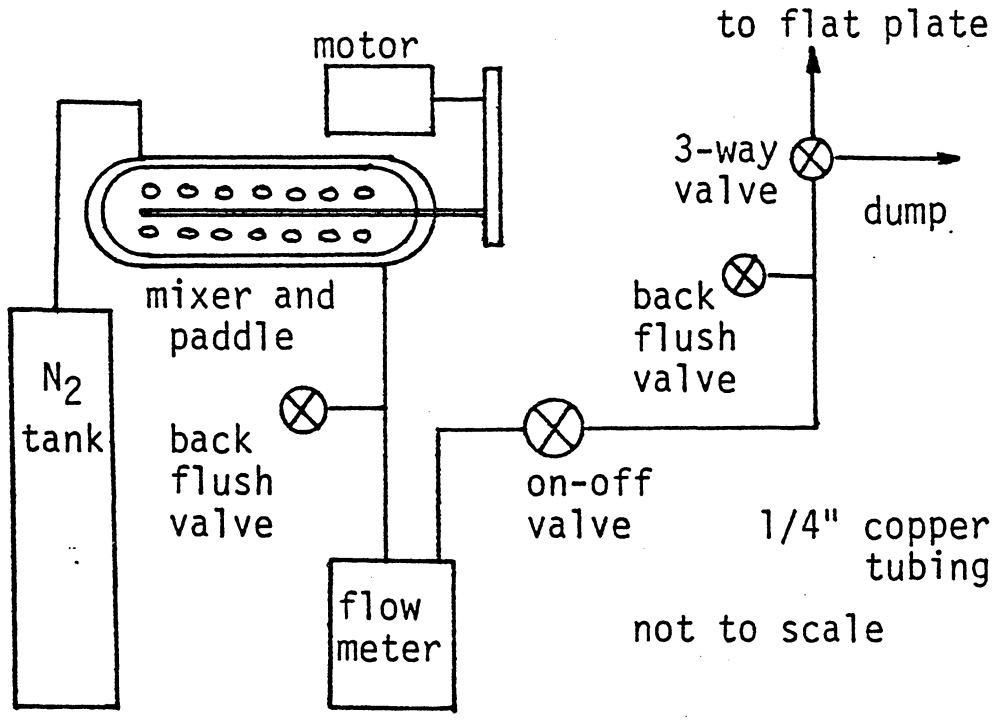

Figure 1: Injection system

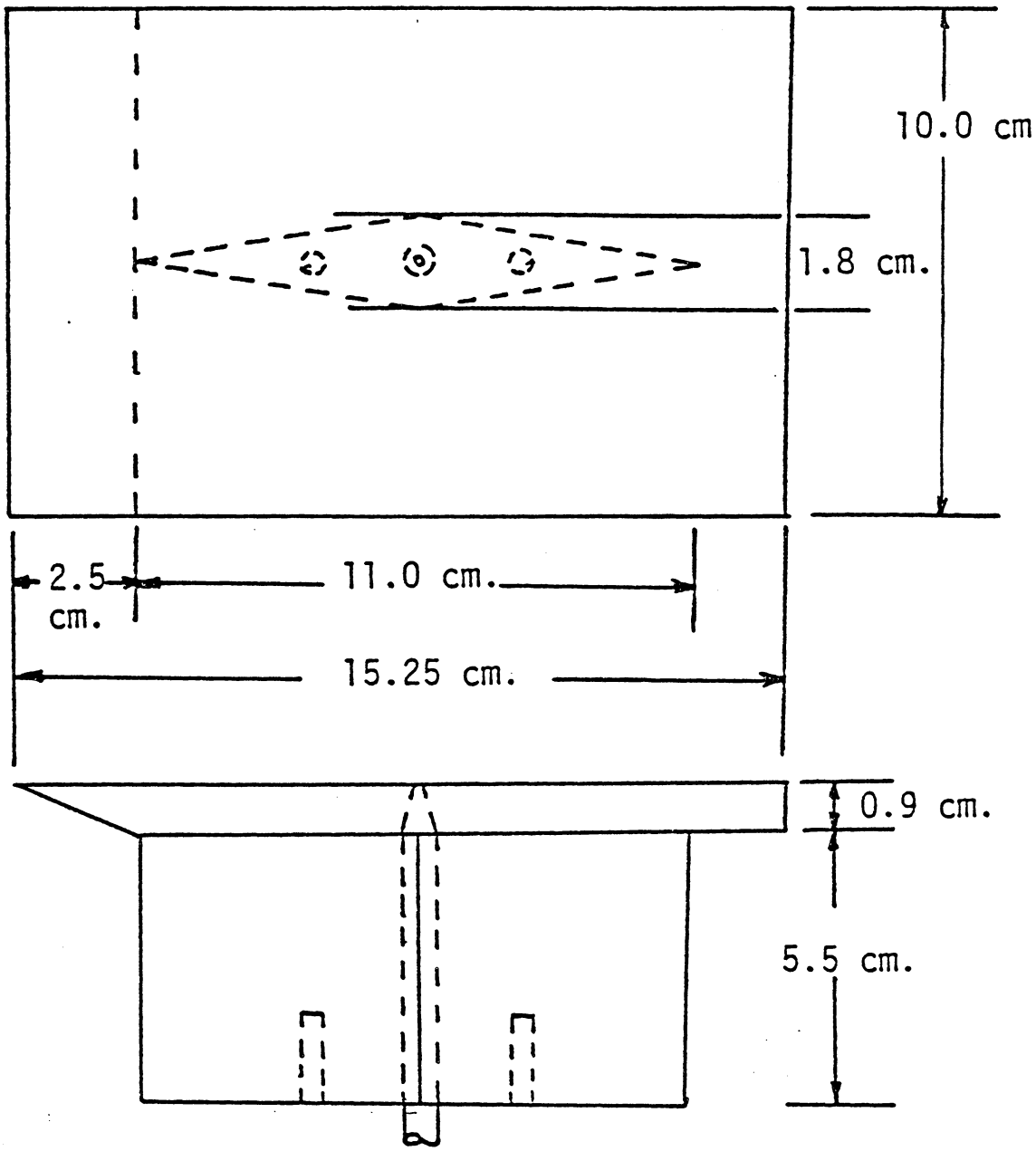

Figure 2: Flat plate model

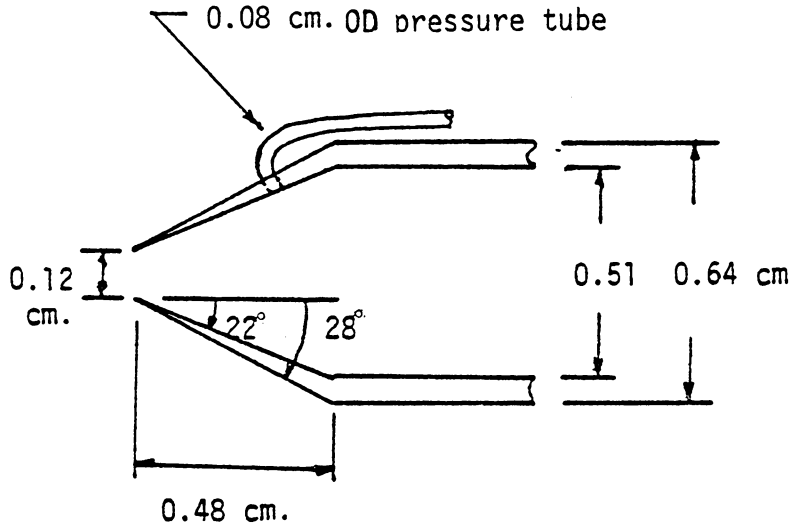

Figure 3: Sampling probe

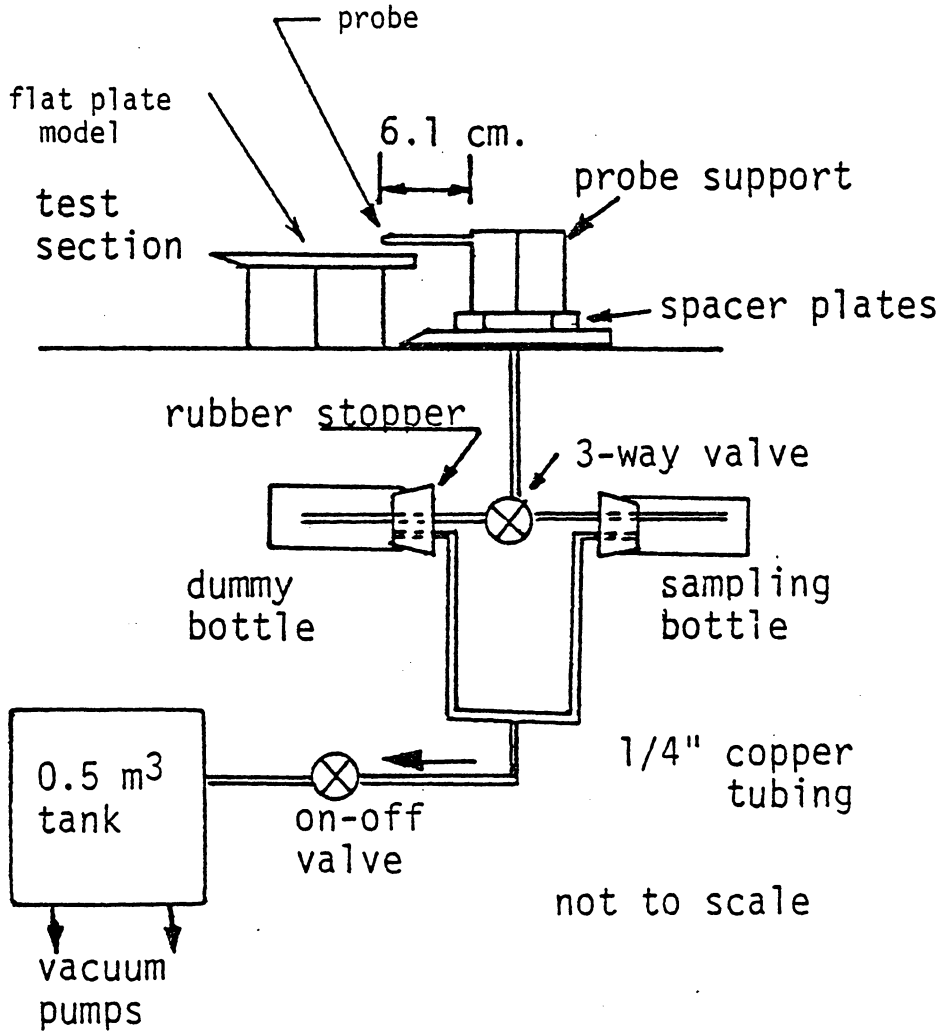

Figure 4: Sample collection system

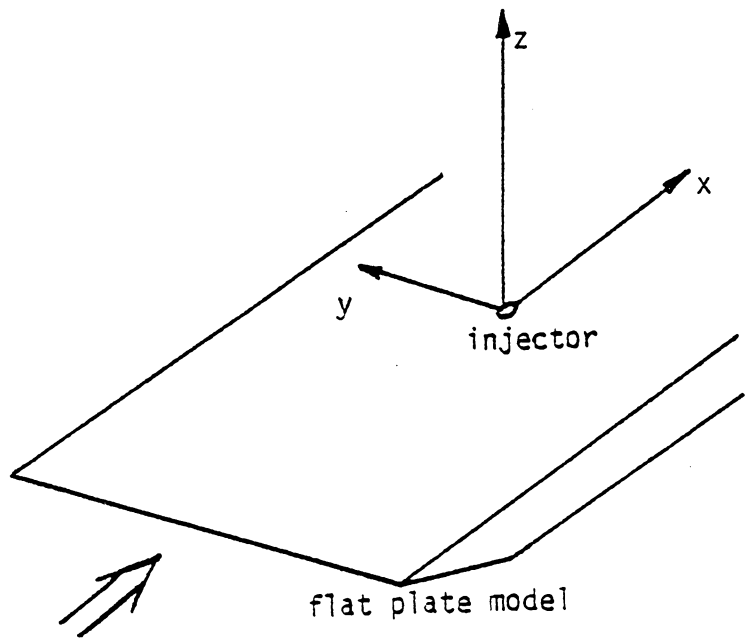

Figure 5: Coordinate system

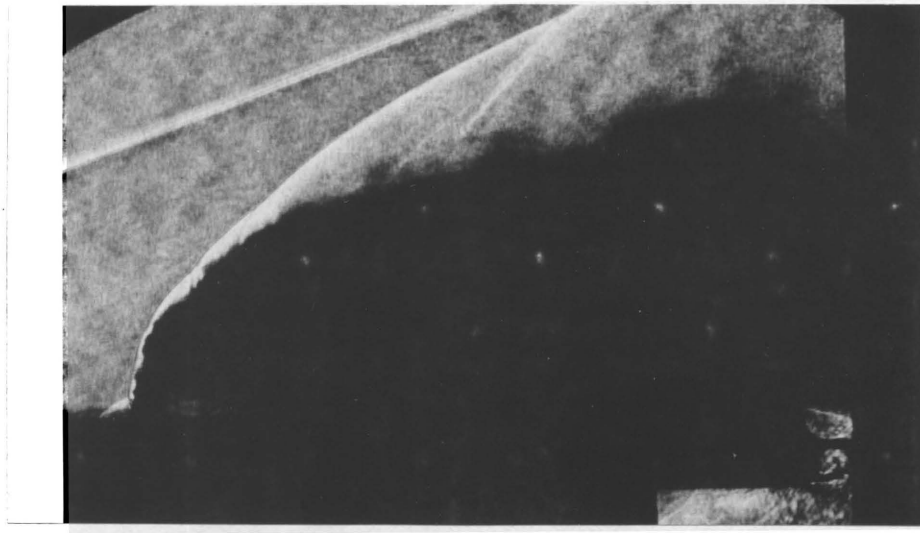

a. Smooth profile

b. Stepped profile

Figure 6: Spark Schlieren photographs of $\bar{q}$=6 liquid jets

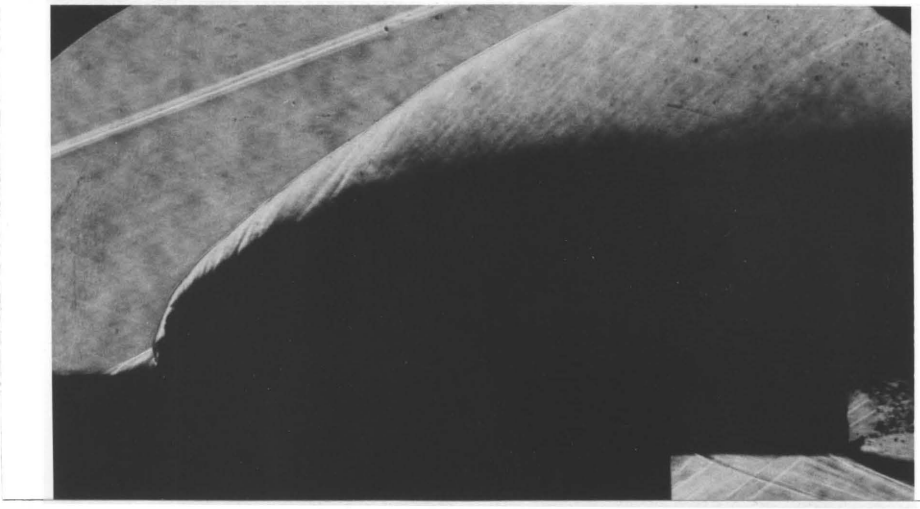

a. Smooth profile

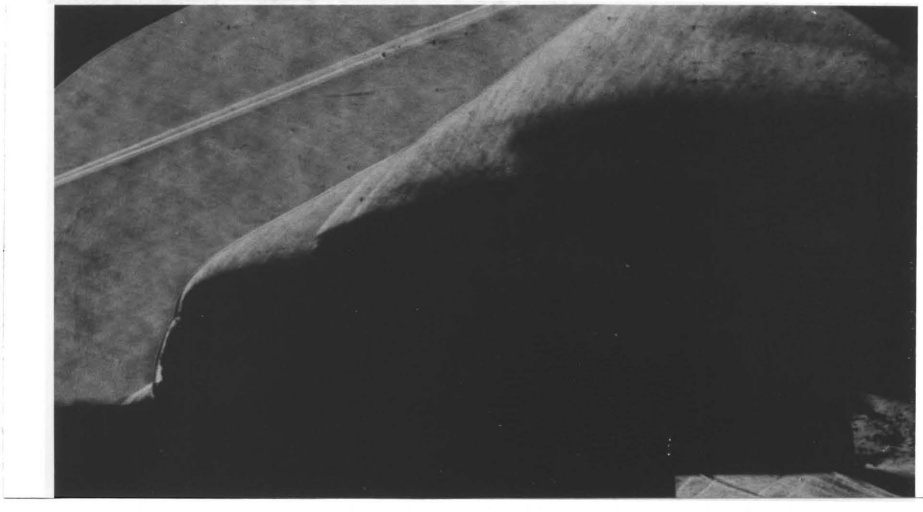

b. Stepped profile

Figure 7: Spark Schlieren photographs of $\bar{q}$=5 slurry jets

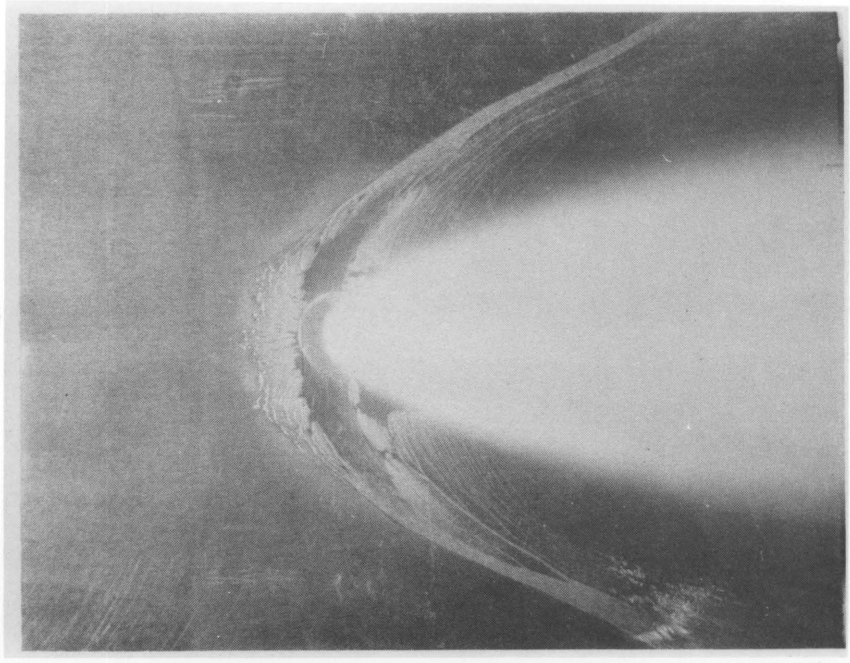

Figure 8: Top view of surface layer of a liquid jet from a 3.2 mm injector at $\bar{q}$=6.1 (Ref. (7))

Figure 9: Front lighted photograph of $\bar{q}$=6 liquid jet and the surface layer

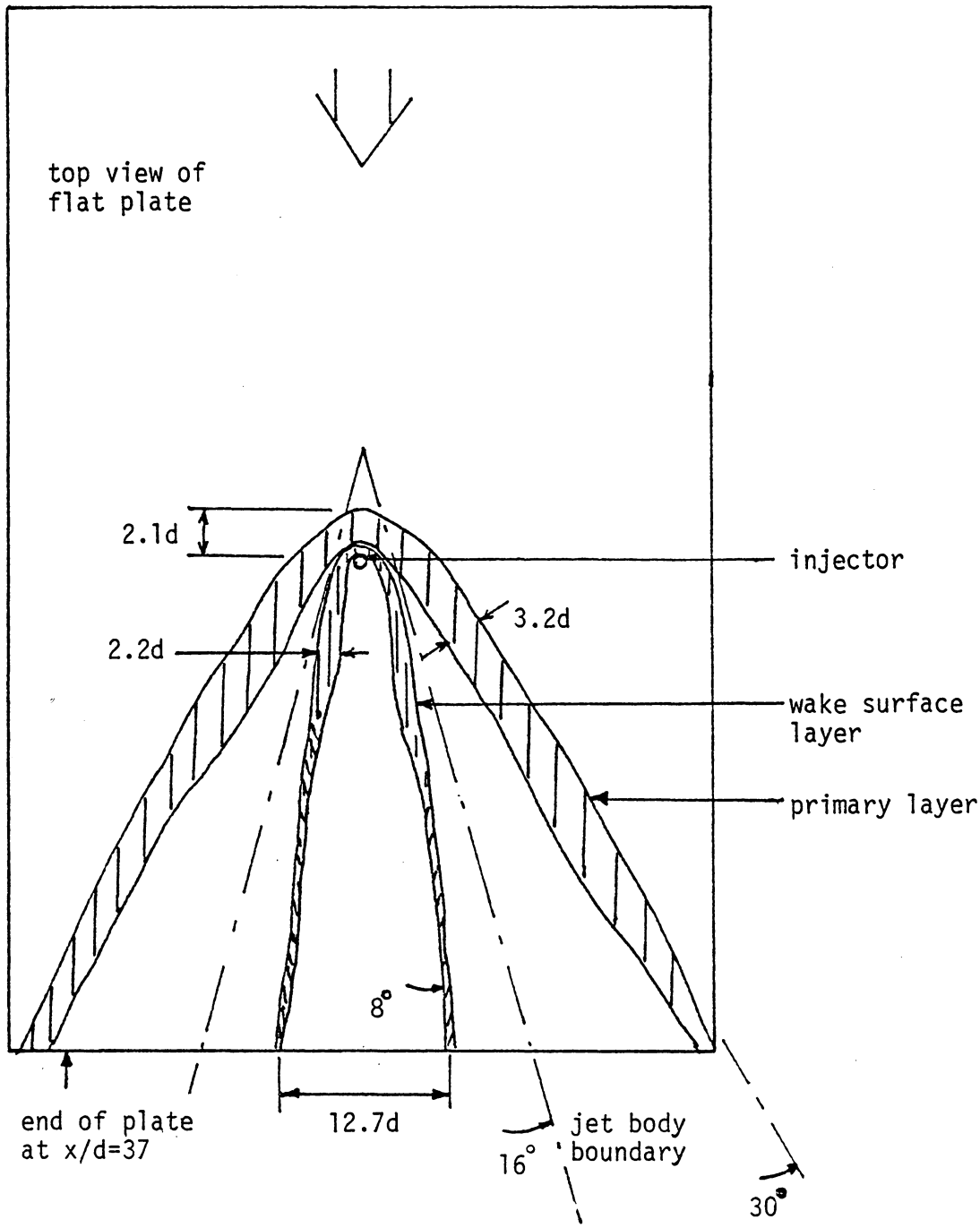

Figure 10: Surface erosion pattern of
$\bar{q}$=6 liquid jet

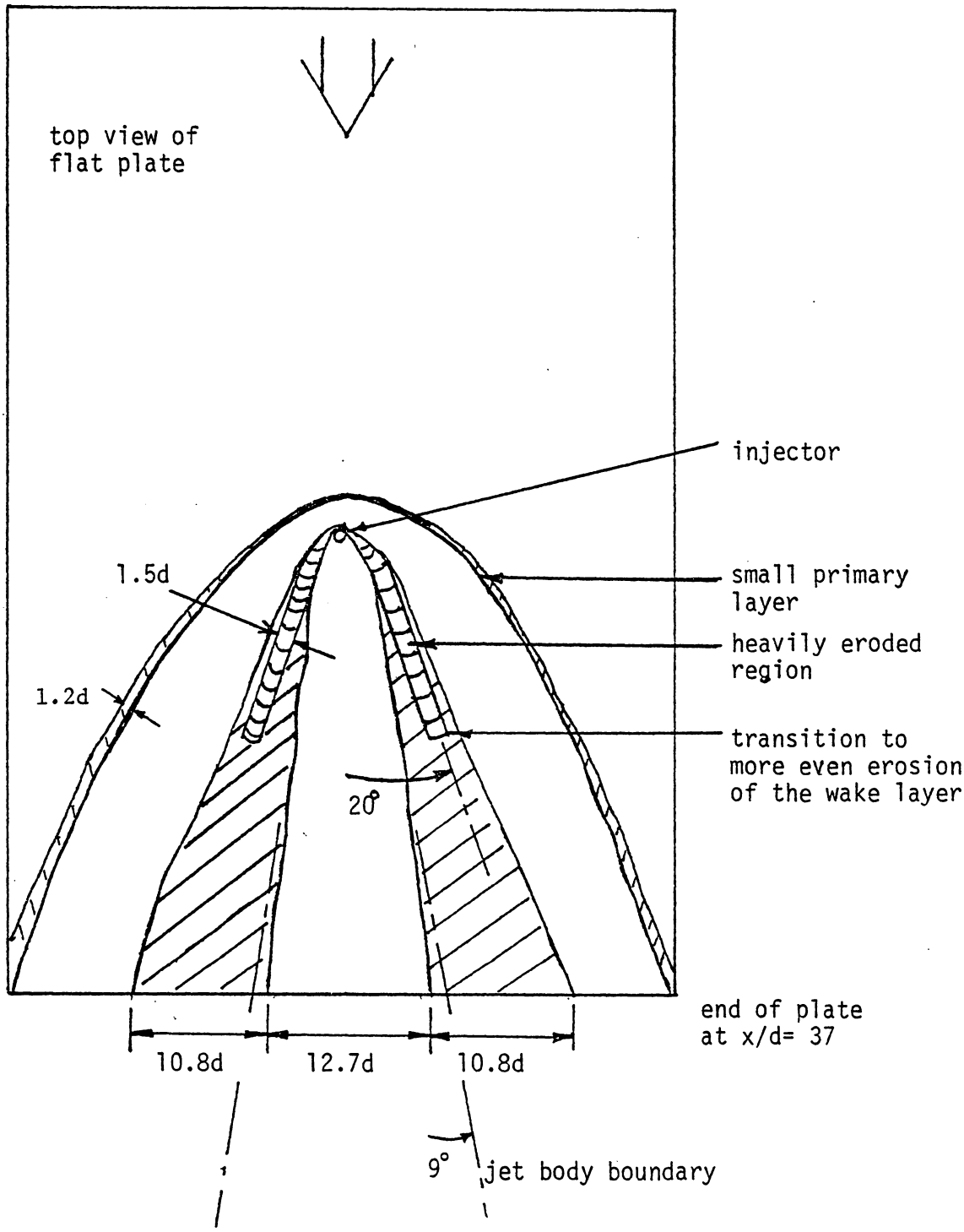

Figure 11: Surface erosion pattern of
$\bar{q}$=5 slurry jet

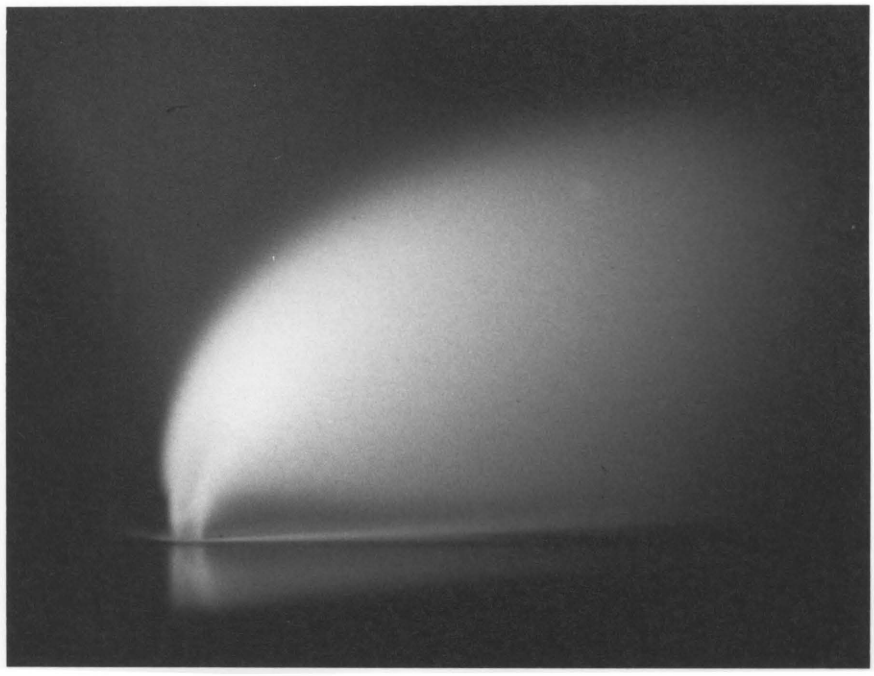

Figure 12: Front lighted photograph of $\bar{q}$=6 liquid jet core and wave strip

Figure 13: Front lighted photograph of $\bar{q}$=5 slurry jet leading edge

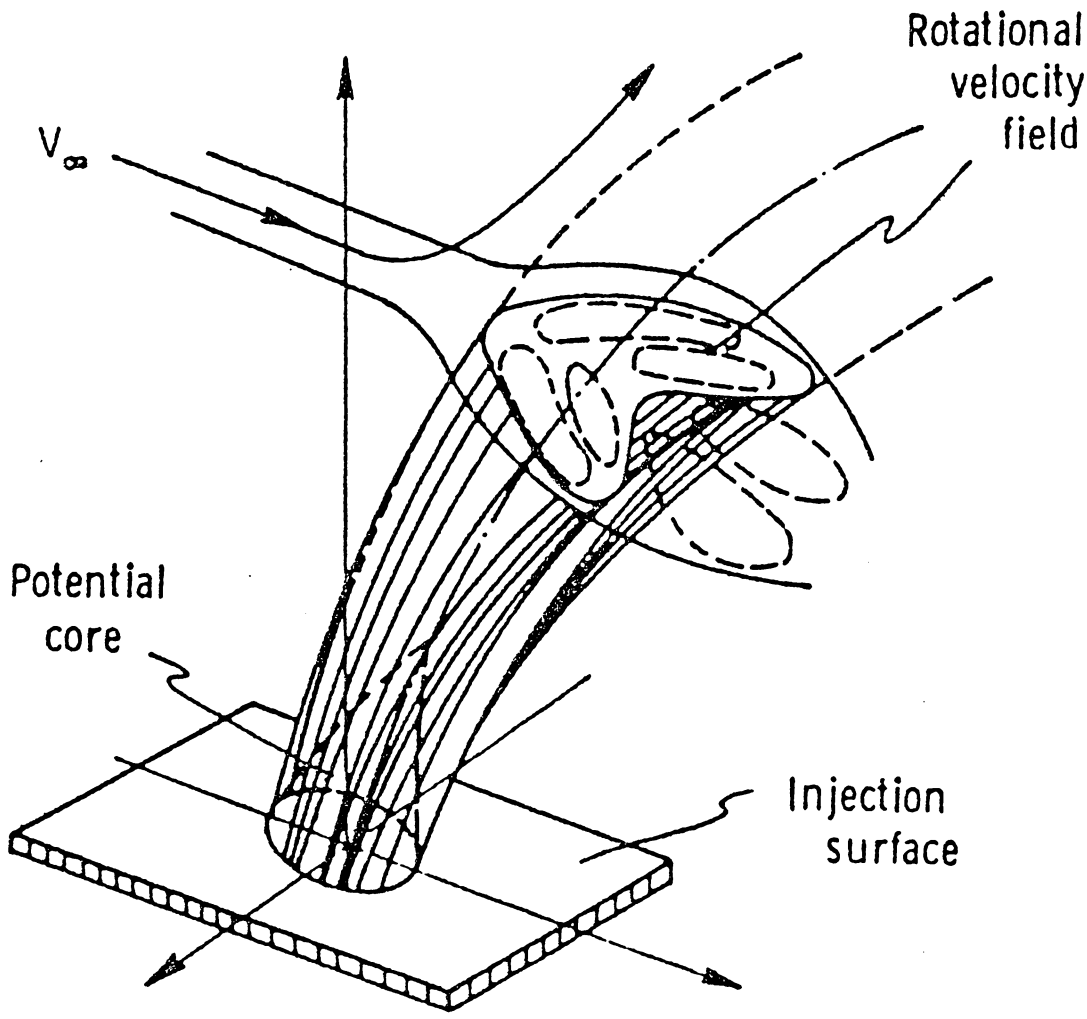

Figure 14: Cross section of jet injected transverse to a subsonic flow (from Abramovich Ref.(17))

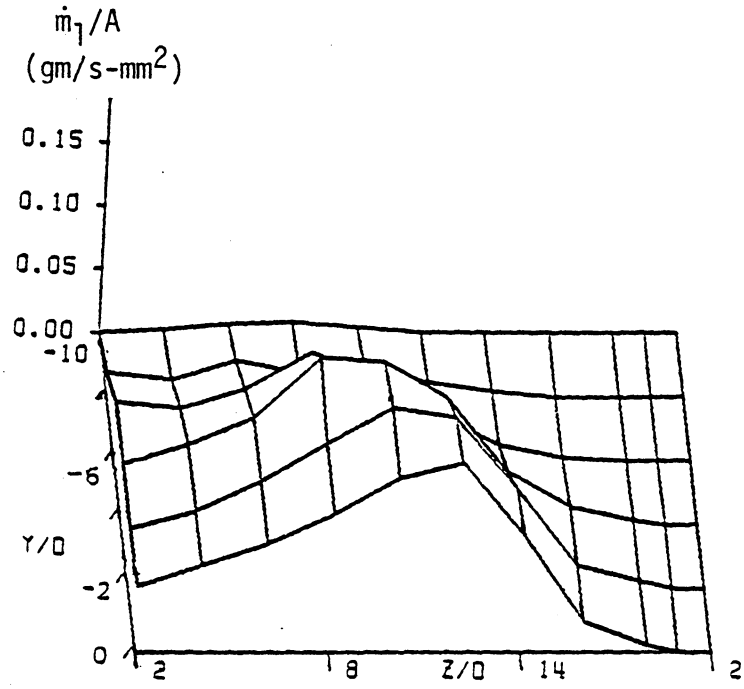

Figure 15a: Graphical depiction of mass flow of liquid per unit area for $\bar{q}$=6 liquid jet at x/d=30

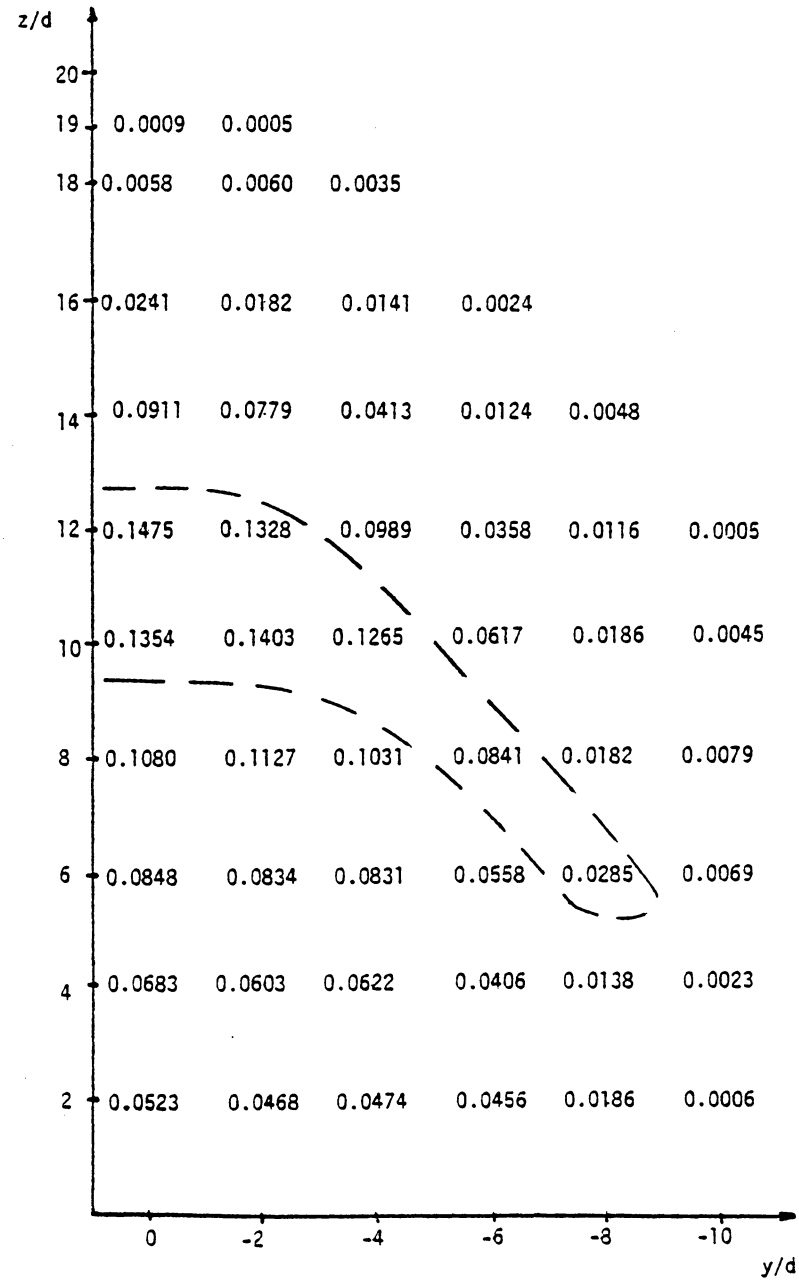

Figure 15b. Numerical values of mass flow of liquid per unit area, $\dot{m}_l/A$ in gm/s-mm^2, for $\bar{q}$=6 jet at x/d=30; enclosed area is the remnant of the kidney shaped main jet body

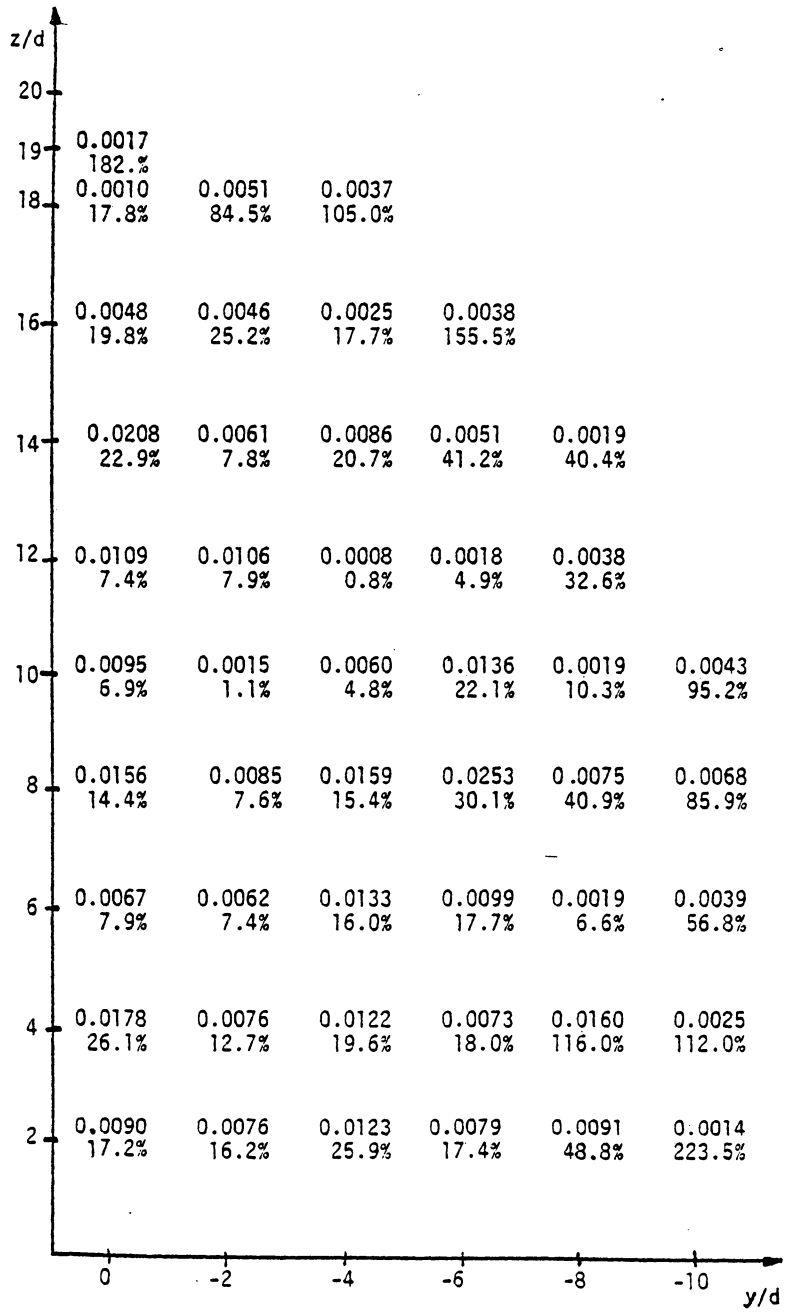

Figure 16: Magnitude of the spread in $\dot{m}_1/A$ in gm/s-mm^2 for the liquid jet, also expressed as a percent of the average value from Fig. 15b.

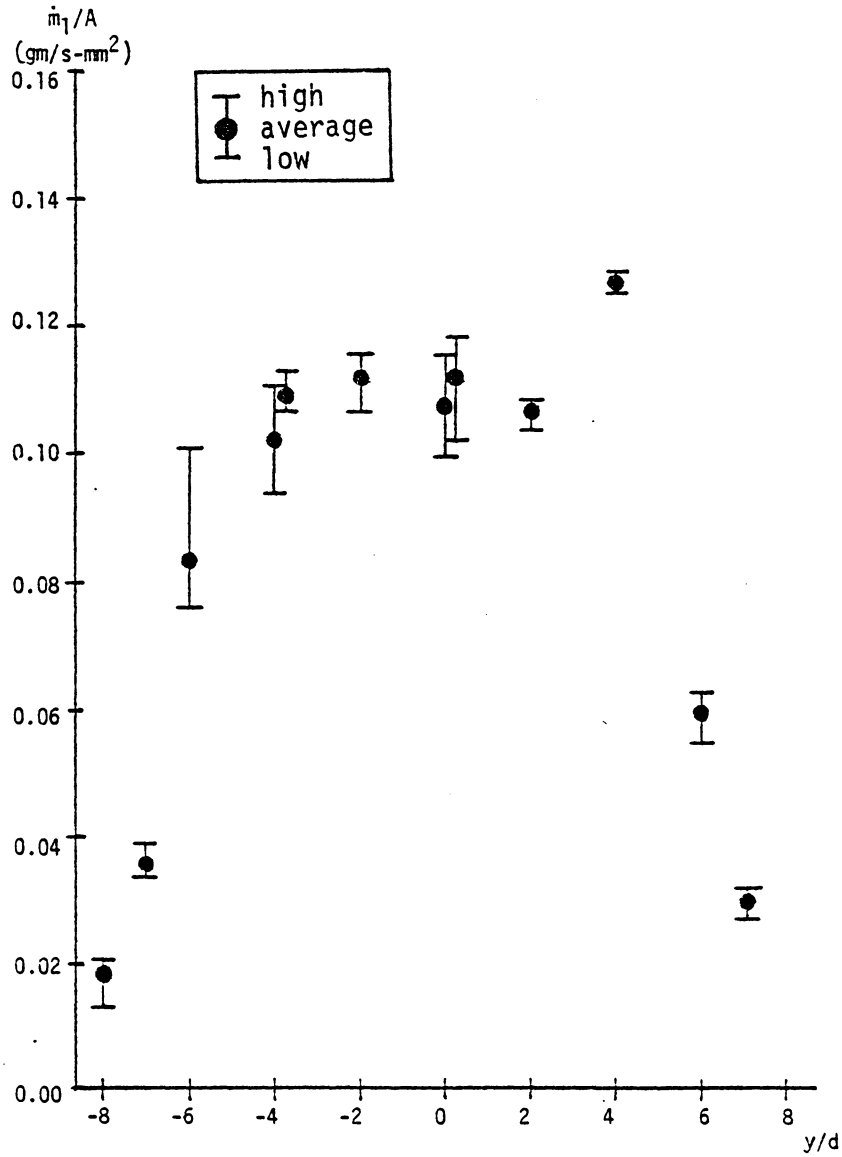

Figure 17a: Mass flow profile for the liquid jet at z/d=8

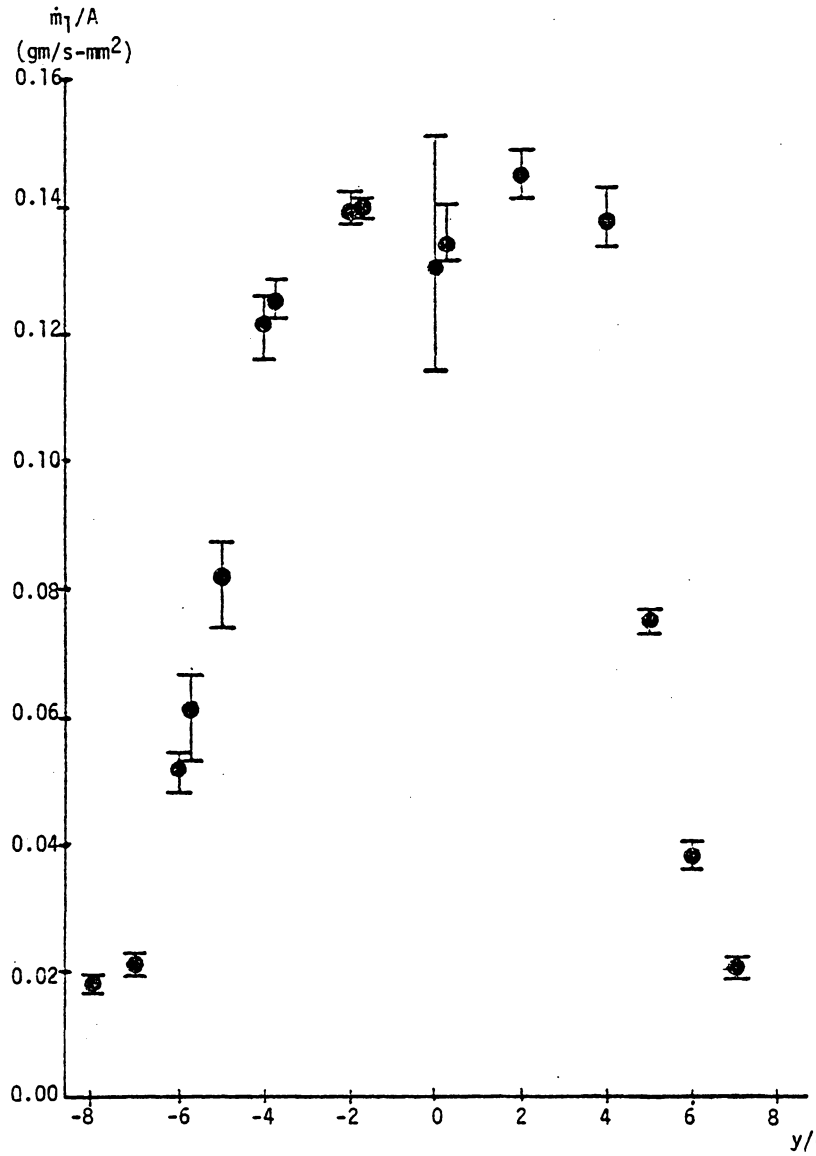

Figure 17b: z/d=10

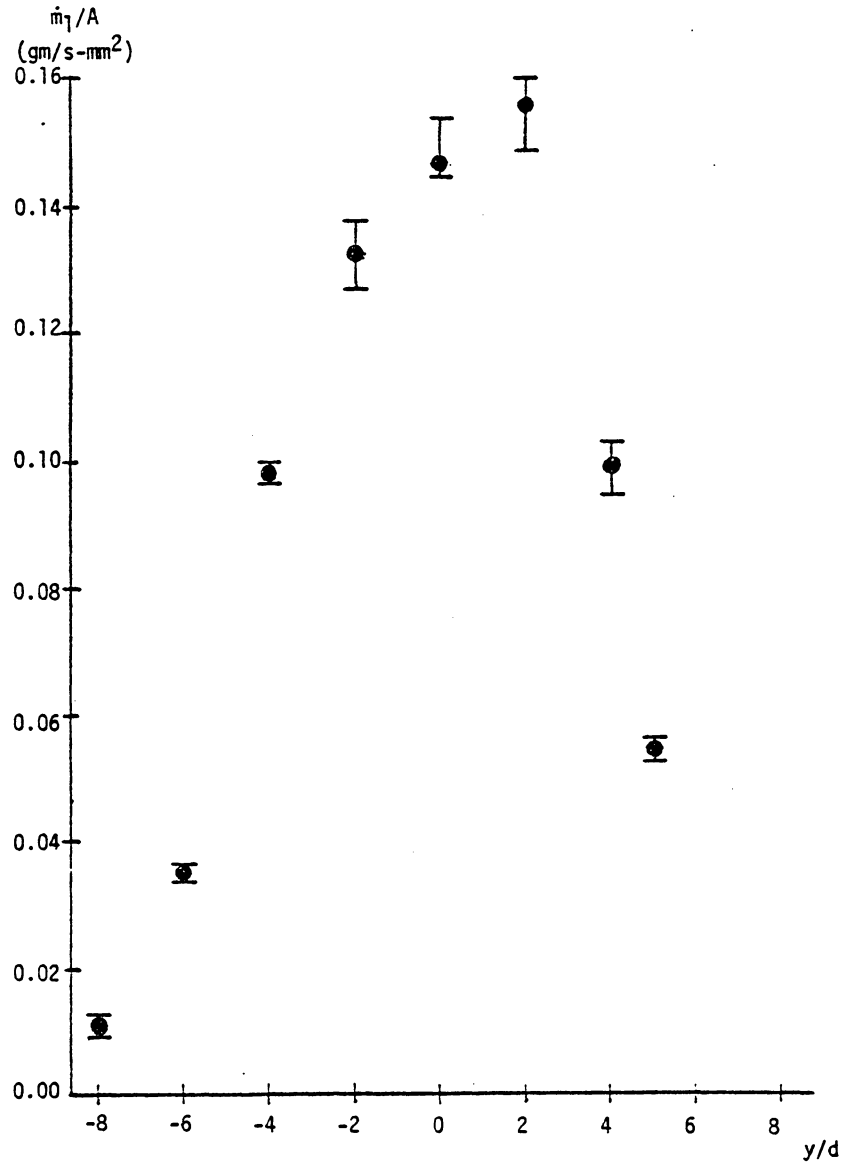

Figure 17c: z/d=12

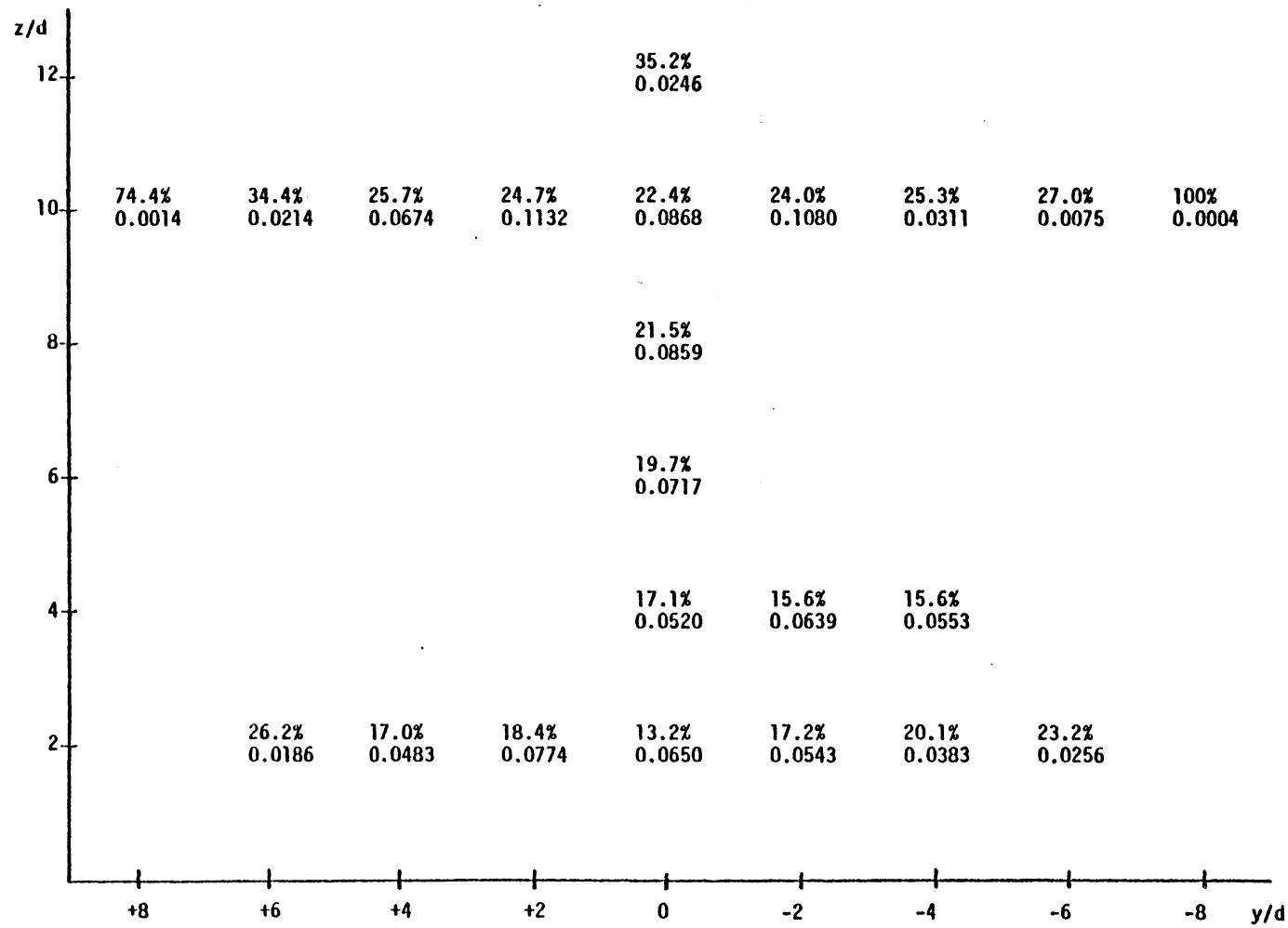

Figure 18: Mass flow of slurry per unit area in gm/s-mm^2 in the x/d=30 plane of $\bar{q}$=5 slurry jet, also the local loading in percent

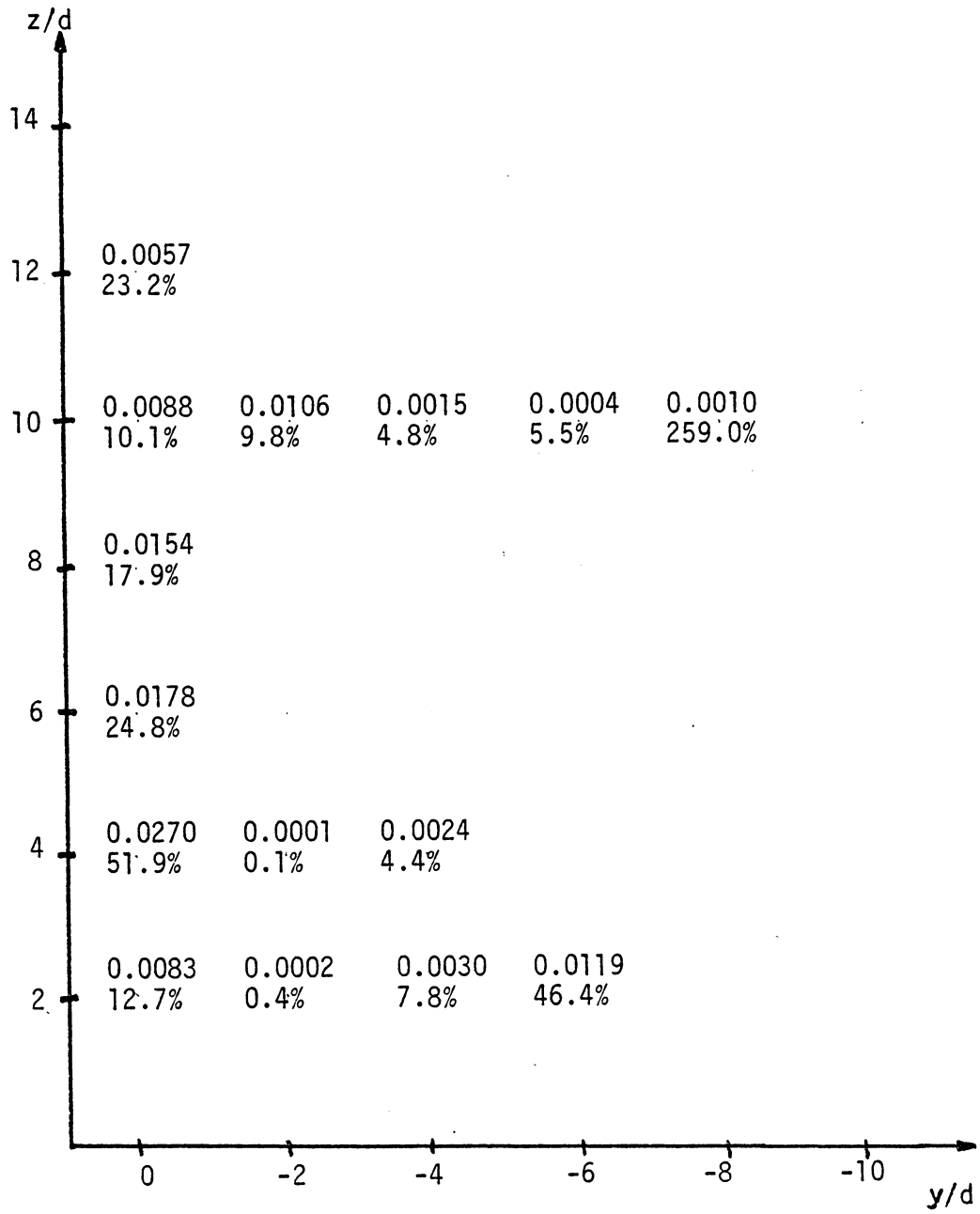

Figure 19: Magnitude of the spread in slurry mass flow in gm/s-mm^2, also expressed as a percent of the average value from Fig. 18

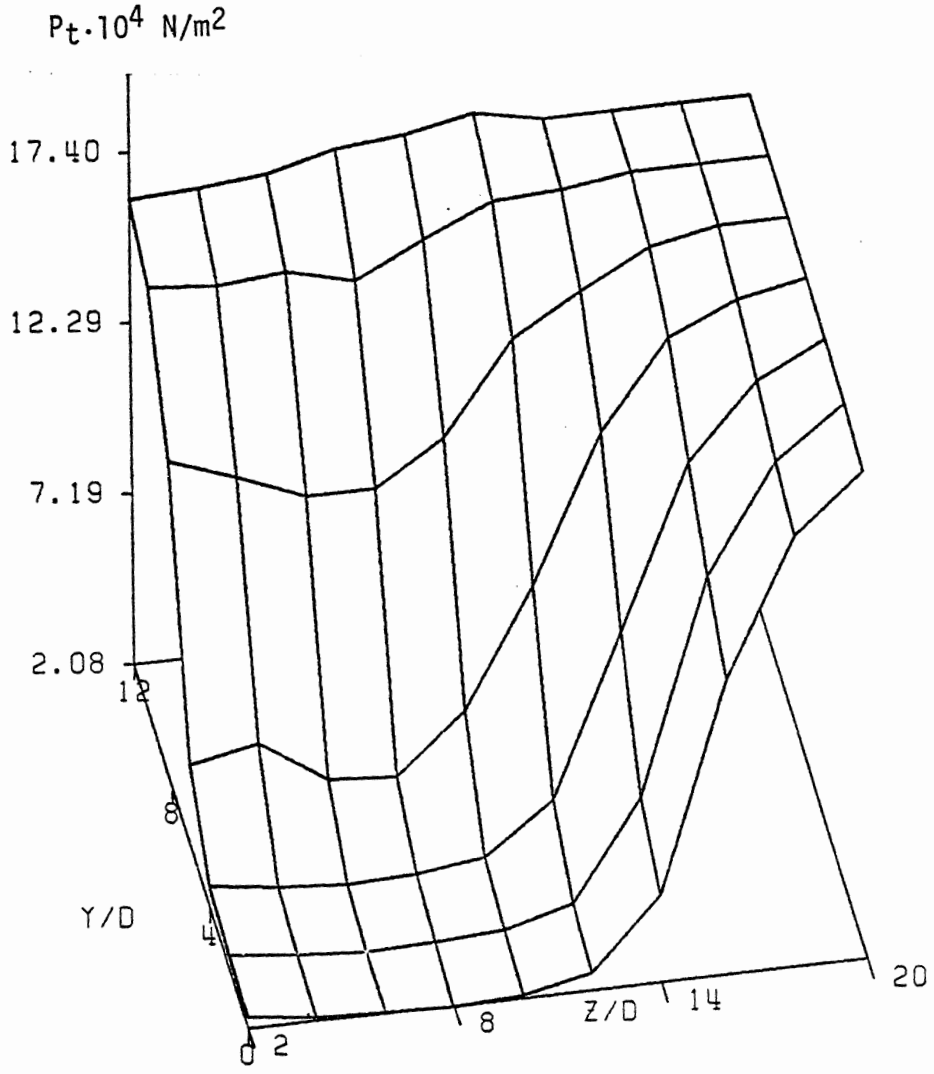

Figure 20a: Graphical depiction of measured Pitot pressures in the $\bar{q}$=6 liquid jet

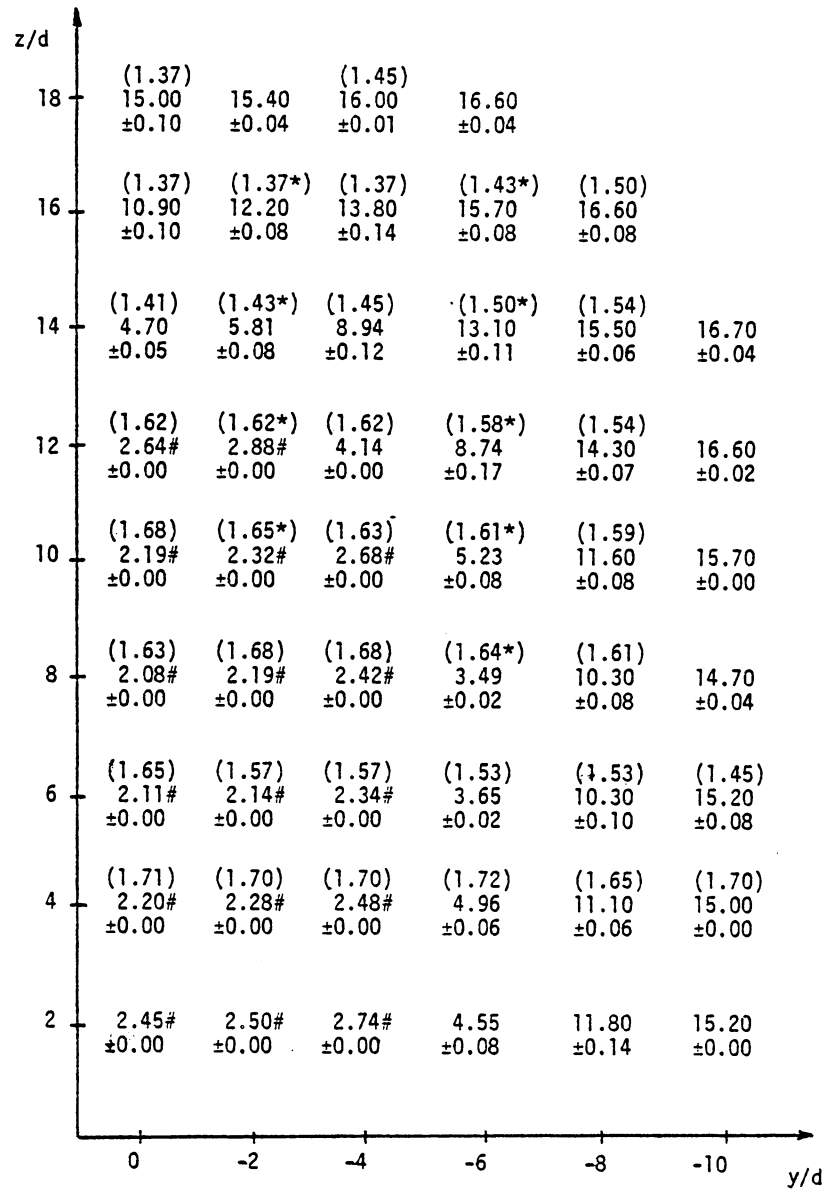

Figure 20b: Pitot pressures P_{t2}, # are P_{t1} ± time variation in P_t, P_s in parentheses; pressures $\cdot(10^4$ $N/m^2)$, * are interpolated P_s values

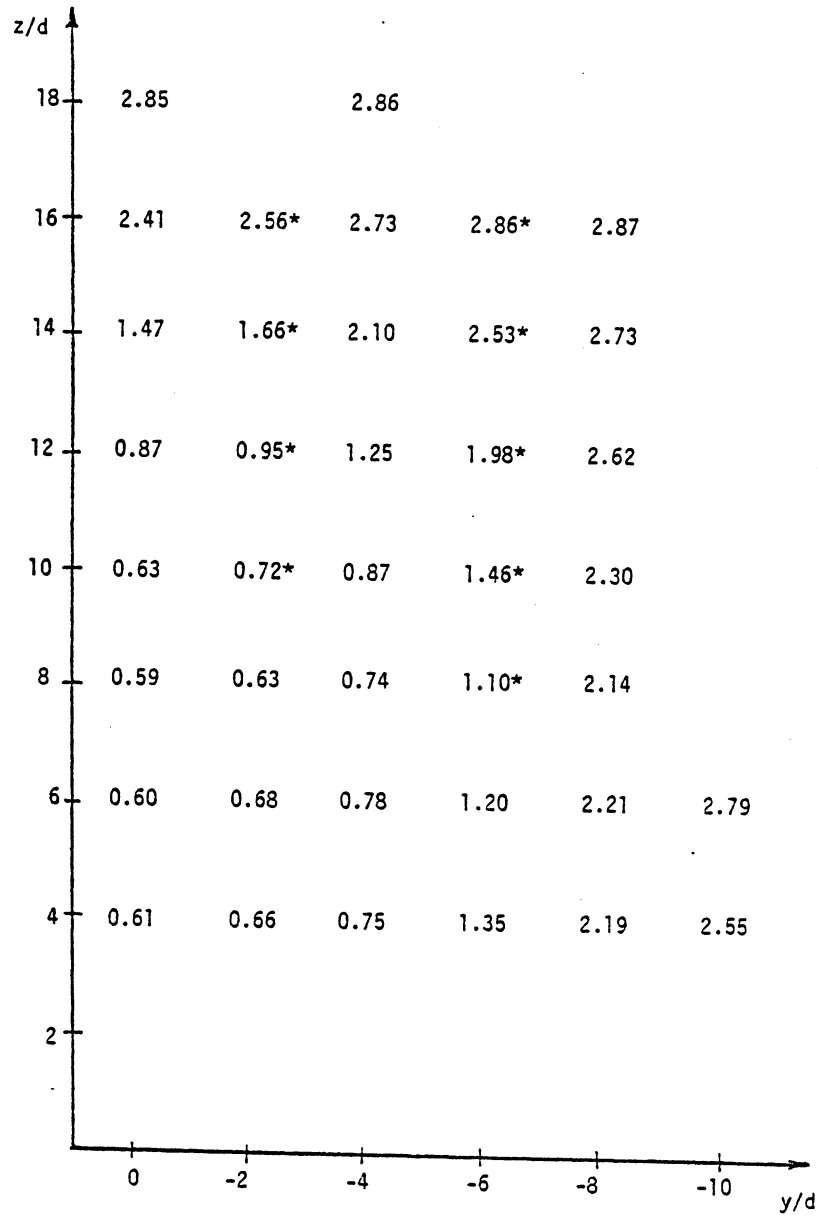

Figure 21: Calculated Mach number distribution; * use interpolated P_s values; liquid jet

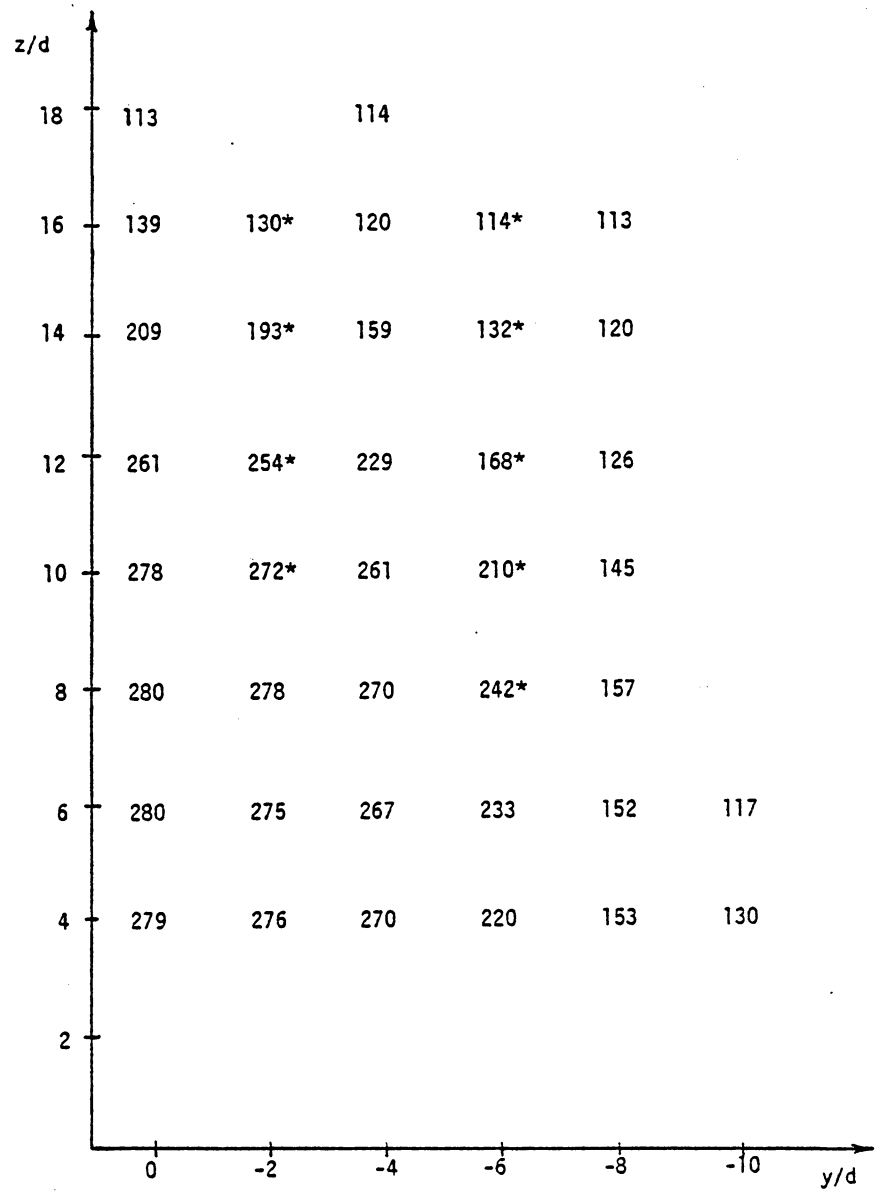

Figure 22: Calculated static temperature distribution; * use interpolated P_S values; $\bar{q}$=6 liquid jet

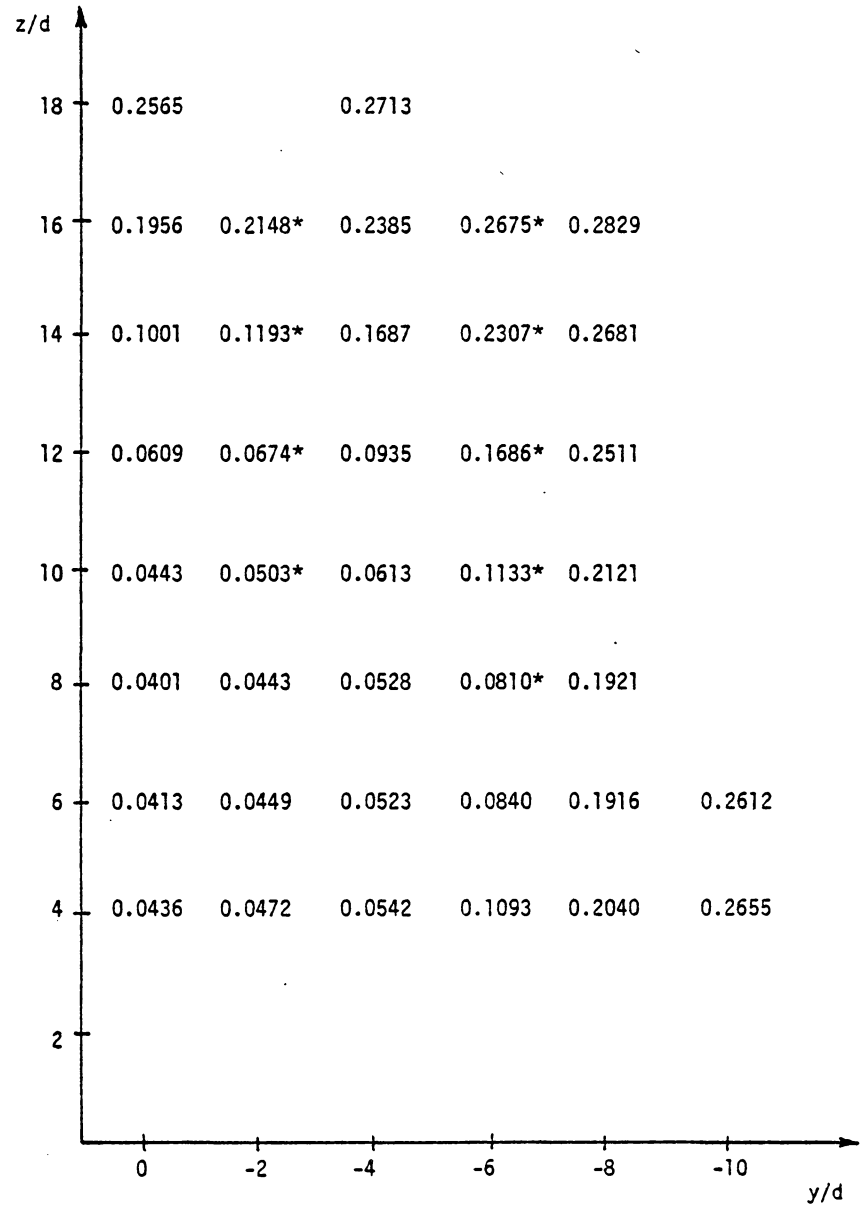

Figure 23: Calculated mass flow of air per unit area, $\dot{m}_a/A$ in gm/s-mm^2; * use interpolated P_s values; $\bar{q}$=6 liquid jet

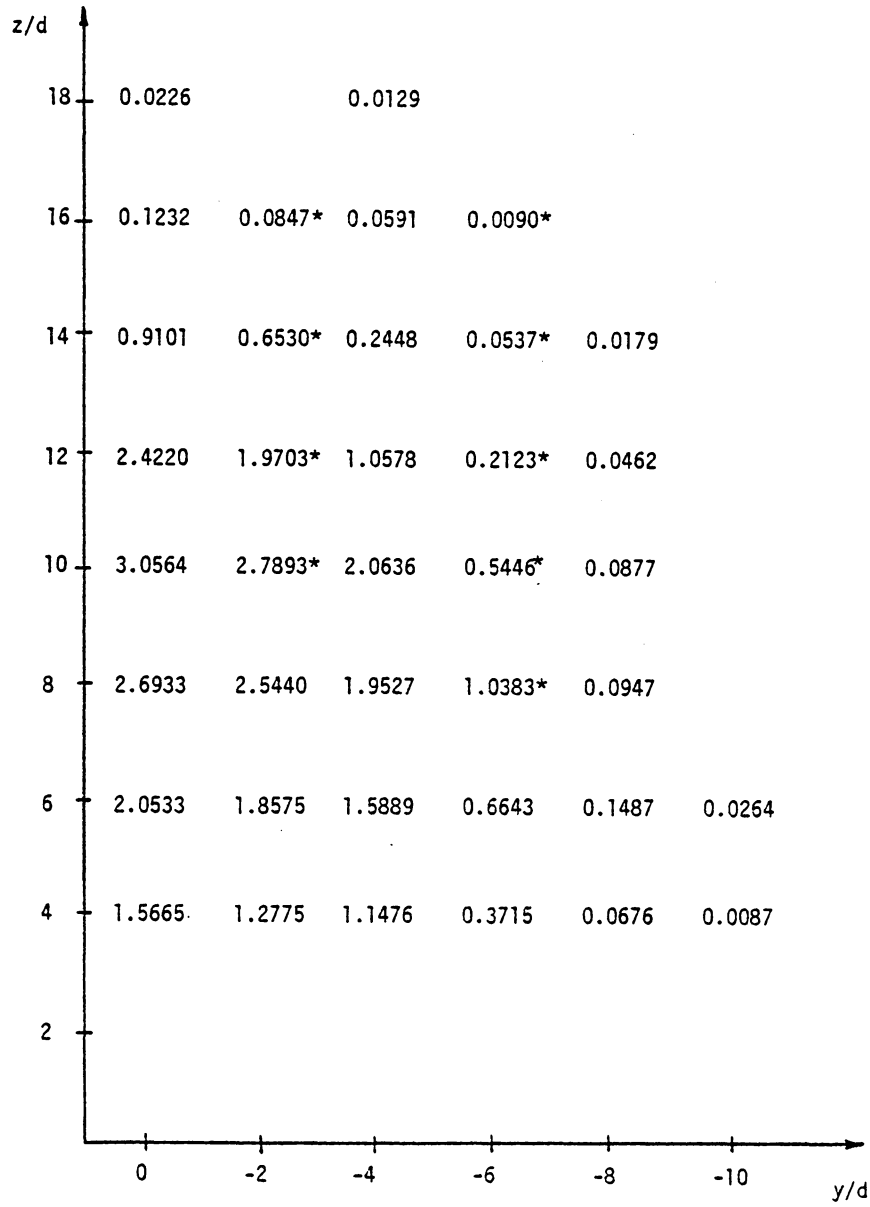

Figure 24: Calculated liquid-to-air mass flow ratio; * values use interpolated P_s values

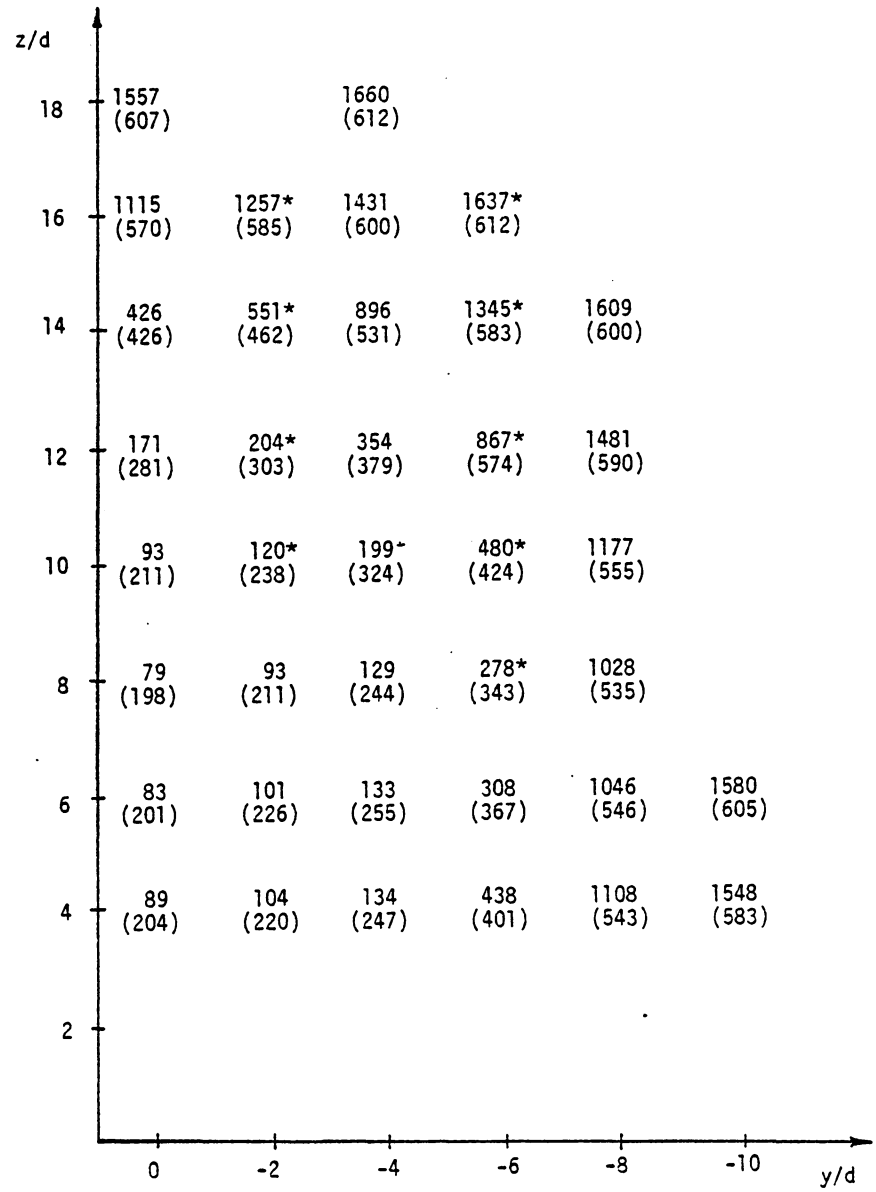

Figure 25: Calculated momentum flux of air, $\dot{m}_a V_a/A \cdot (10^2)$ gm/mm-s^2; velocity of air, V_a m/s, in parentheses; * use interpolated P_s values

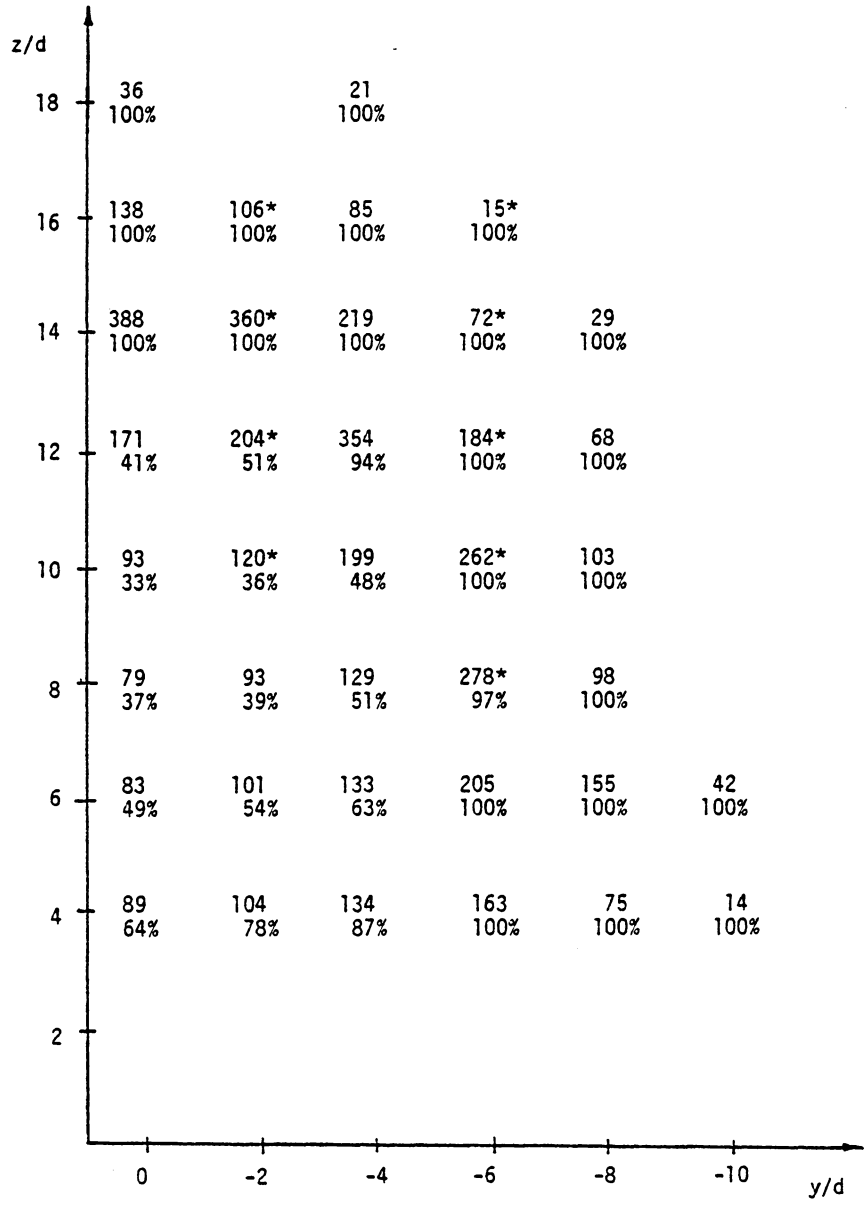

Figure 26: Calculated momentum flux of liquid, $\dot{m}_l V_l / A \cdot (10^2)$ gm/mm-s^2; velocity of liquid as a percent of local air velocity;
* use interpolated P_s values.

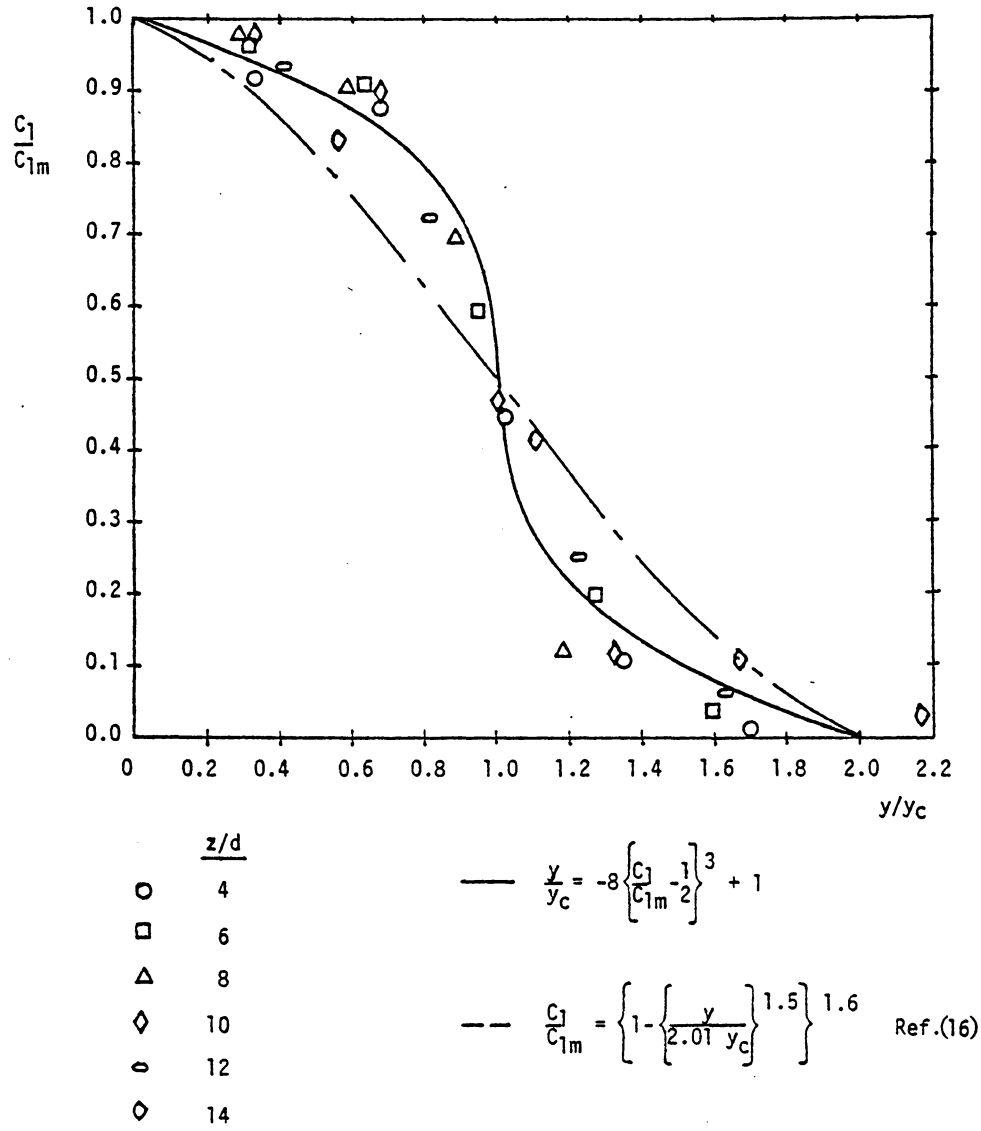

Figure 27: Liquid concentration data and correlations for $\bar{q}$=6 liquid jet

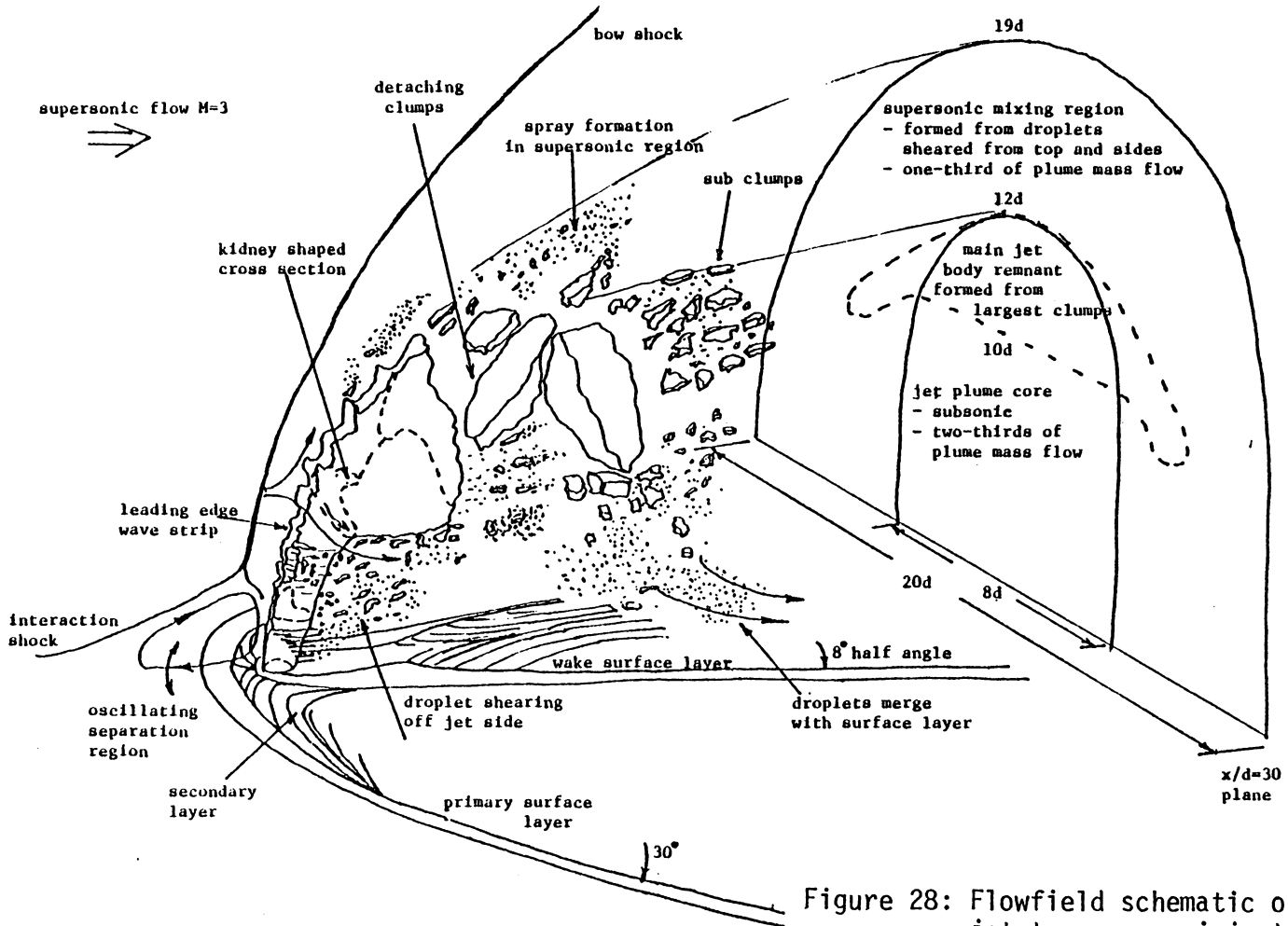

Figure 28: Flowfield schematic of liquid jet transverse injection in Mach 3 airflow from orifice of diameter d

The vita has been removed from the scanned document